Spring 2015

Signal integrity analysis of a low cost PCB to PCB system

Kancy Robison

Department:

SIGNAL INTEGRITY ANALYSIS OF A LOW COST PCB TO PCB SYSTEM

by

KANCY ROBISON

A THESIS

Presented to the Faculty of the Graduate School of the

MISSOURI UNIVERSITY OF SCIENCE AND TECHNOLOGY

In Partial Fulfillment of the Requirements for the Degree

MASTER OF SCIENCE

in

ELECTRICAL ENGINEERING

2015

Approved by

James Drewniak, Advisor

Jun Fan

Daryl Beetner

ABSTRACT

This report presents the analysis of a low cost PCB to PCB cable and connector system focusing on its data rate limitations and optimizing transmitter and receiver operations. Economic factors have an ineluctable presence in digital hardware engineering, and as data rates are continually pushed to new bounds, finding cheap alternatives to boost performance in digital systems is of great practical concern. This study will show the measurement and simulation of a digital system which includes a PCB board, connector, and a multi-pin flex cable (ribbon cable). These results will then be used to optimize performance via receiver and transmitter operations such as equalization.

ACKNOWLEDGMENTS

I would fist like to acknowledge Dr. Drewniak for his support and guidance throughout the completion and writing of this thesis. I would also like to thank my other committee members for taking the time to proliferate over my defense, and for the knowledge gained in their courses.

Some others I would like to thank are some of my closer friends including Kyle Williams, Tom Walters, and Koyel Banerjee. And I would also like to thank my Mother.

TABLE OF CONTENTS

Page

LIST OF ILLUSTRATIONS

Page

LIST OF TABLES

Page

1. INTRODUCTION

Digital systems offer many challenges to electrical engineers. Often times, digital systems are simplified through the abstraction of symbolization. However, when data rates become very high and resulting wavelengths are small relative to the physical dimensions of components in the system, this symbolization is often unable to accurately predict performance. When this happens, digital signals are treated as analog signals and transmission line theory must be used to characterize the performance of a system. This subset discipline of electrical engineering is called signal integrity, and is concerned with the performance of a digital system in relation to its physical dimensions, spectral content, and temporal properties.

In this thesis a low-cost digital system, as demonstrated by Figure 1.1, is examined with a focus on signal integrity analysis, simulation, and optimization. This thesis will walk through the process of characterizing the system in the frequency and time domain through using a time domain reflectometer and network analyzer. It will briefly describe these measurements as well as the calibration and de-embedding techniques used. Next, the system will be simulated using arbitrary transmission line simulators and full wave solvers. This simulation process is performed in an effort to gain an intuitive insight to how the various physical and electrical characteristics of the system affect performance parameters. It will close with the optimization of the system using well known transmitter and receiver techniques: passive continuous time linear equalization; decision feedback equalization; and transmitter de-emphasis.

Overall, this thesis can give insight into how well a low cost system can perform. And what methods can improve its performance with some engineering. This is a very common problem in engineering as economics are often the driving force behind real world design decisions.

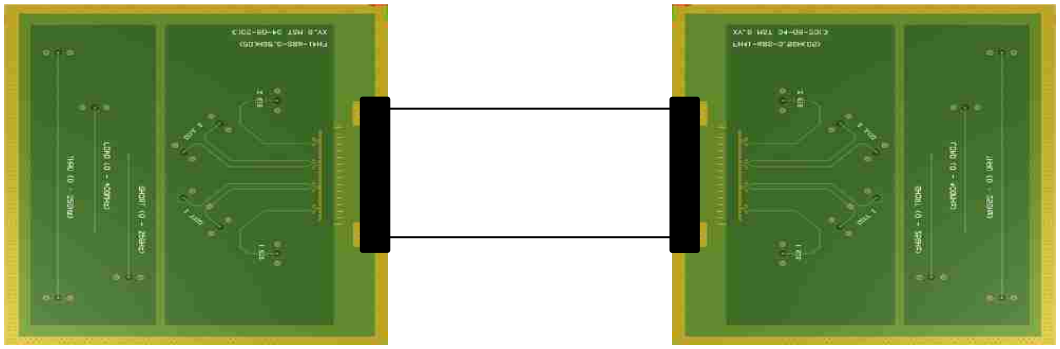

Figure 1.1 Pictorial representation of low-cost digital system studied

2. METHODOLOGY

This project has three main components, the characterization or analysis of the PCB to PCB system, its modeling and simulation, and finally its optimization using transmitter and receiver techniques. This section will outline the methodology for each of these components but will first focus on giving more detail on the system used.

This system is typical for many low cost applications. Essentially, it is made up of a PCB using FR4 dielectric and a microstrip trace. This trace leads to an SMA adapter on one end and to a Hirose Fh41 flex cable connector [1]. Next, a Nicomatic flex cable [2] is used to bridge two PCBs using the Hirose connectors. A detailed representation of the system is shown in Figure 2.1. There are many design variations within this system. One variation is the signaling type found on the PCB board, where both single-ended and differential signaling types can be found. There is also a great amount of variation found in the flex cables used in the system: single-ended and differential signaling; microstrip and stripline geometries; varying lengths of three, six, and twelve inches. A chart of the various flex cable design variations is in Table 2.1.

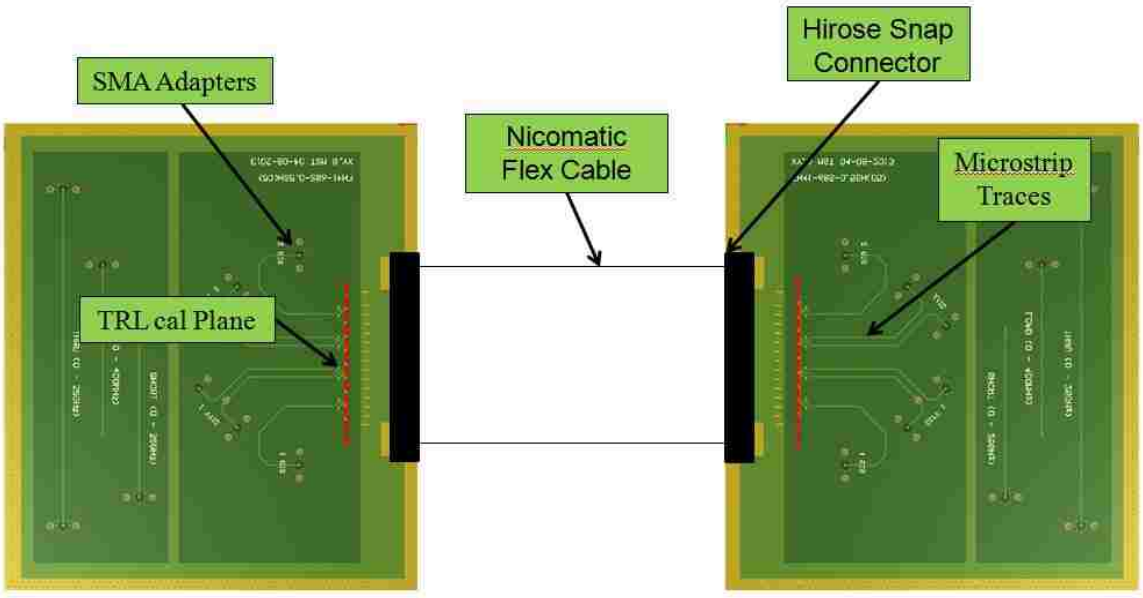

Figure 2.1 Detailed representation of the low-cost digital system used in study including labeled subsystems

Table 2.1 Table of studied cable design variations

	3 In.		**6 In.**		**12 In.**	
Microstrip	SE	DIFF	SE	DIFF	SE	DIFF
Stripline	SE	DIFF	SE	DIFF	SE	DIFF

Anytime a new system is developed its performance must be characterized and put into known and well defined parameters. Typically in signal integrity engineering, all three domains are investigated: the frequency domain; time domain; statistical domain.

The system can be studied in the frequency domain through use of network parameters which can be measured via a PNA (performance network analyzer) or VNA (vector network analyzer) [3]. In this study, a VNA was used to capture S-parameters up to 25 GHz for each of the flex cable design variations. For the single ended case, a TRL calibration was used in order to better capture the effect of the flex cable and Hirose connectors on the performance of the system. As a differential TRL does not exist, a simple calibration was used at the end of high performance cables used in the measurement of the differential S-parameters.

Typically the technique of TDR (time domain reflectometry) [4] is used to analyze the transient properties of a system. For this study a TDR was used for the time domain measurement of this system. TDR is often used to find the spatial location of transmission line discontinuities, and to determine the inductive or capacitive effects of these discontinuities, allowing for an intuitive understanding of the physical properties of the channel.

Finally, the statistical domain of the system is often characterized by the use of eye diagrams [5], which are essentially created by sending pseudo-random sequences of symbols though the channel, and then overlaying the response of all of these symbols on top of each other. This method gives insight into how the channel's impulse response affects performance for the many possible symbol combinations that could be found in practical usage. Oftentimes, eye diagrams will be measured through the use of an oscilloscope. However, equally useful results can be found by simulation using measured S-parameters, this is the technique used in this study.

The next important step is the development of a model. This process provides many benefits to an engineer. First, it helps the engineer to gain a grasp on how different design variables, most notably electrical and physical parameters, have on the overall results seen in the

characterization of the system. Also, it gives the engineer a platform by which experimentation and optimization can be performed on the system. It can also help to correlate measurements to simulations.

For this project, the use of arbitrary transmission line simulators and full-wave simulators are used. The system was essentially broken into three parts, two parts being the PCB trace to Connector with a small snippet of flex cable and the other part being the rest of the flex cable. Figure 2.2 shows the arrangement of the three subsystems.

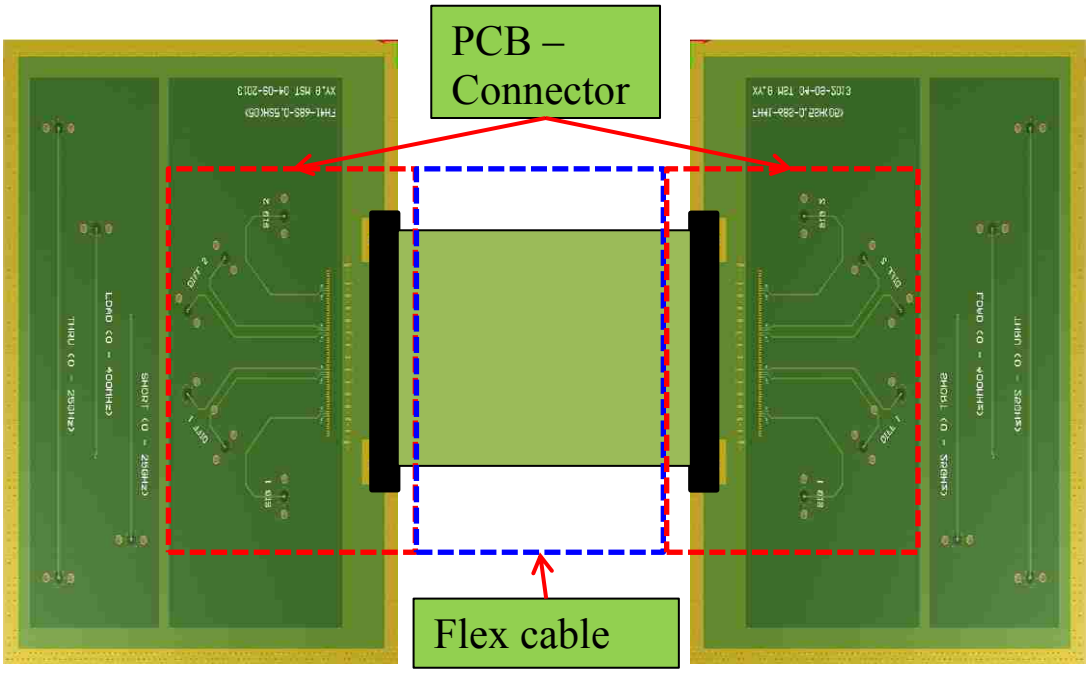

Figure 2.2 The three sub-systems used for simulation and correlation of s-parameters

For the PCB connector portion, CST's full wave time domain solver [6] was used. This was chosen due to its complicated geometry and many discontinuities. The full wave modeling tool gives the flexibility in the 3D drawing phase to accurately represent the connector and

transition in the most realistic way possibly. And as a field solver, calculates the system without the quasi-static assumptions found in the transmission line modeler. A small portion of the flex cable is included in this model, as this allows for the combination of the three sections in a system by insuring that the field distribution connecting the PCB-Connector component and Flex cable component are both TEM and both satisfy the quasi-static assumptions for that connection.

The flex cable is portion is modeled in an arbitrary transmission line simulator. This simpler and faster simulation approach can be used because the majority of the flex cable is essentially a uniform transmission line, and the sections of the flex cable with more complicated current and field distributions are modeled in the full wave modeler. Using both these tools, S-parameters can be calculated and exported to be used in other simulators for analysis and design purposes.

With the S-parameters for each sub-system are found, it is simply a matter of properly cascading the matrices to find the S-parameters for the entire system. Care must be taken to order the ports in the correct way during cascading, shown in Figure 2.3. In this setup the PCB-Connector model S-parameters only need to be calculated once but cascaded twice, so therefore one subsystems' ports must be treated in the opposite order when cascading.

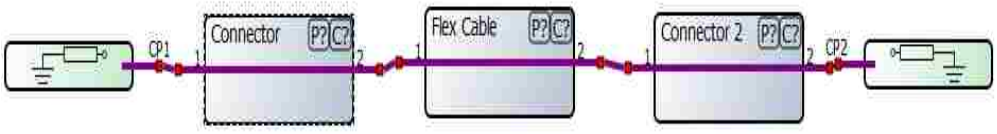

Figure 2.3 Cascaded S-parameter setup in FEMAS tool of three sub-systems

Once the system is characterized and a readily modifiable model is available, the next step in the process is to perform optimizations on the system. There are many possible ways to optimize a system like this for signal integrity. In this project it was assumed that the engineer would have no control over physical and electrical parameters. This basically leaves the transmitter and receiver to have the primary role in channel performance improvement. Three transmitter and receiver signaling schemes are explored in this work: passive CTLE (continuous time linear equalization); transmitter de-emphasis; and receiver DFE (decision feedback equalization).

CTLE is often thought of as a frequency domain solution [7]. A typical S-parameter response found in many systems is a roll off effect at higher frequencies as seen in Figure 2.4. This higher energy spectral content can cause inter symbol interference (ISI). For data rates with Nyquist frequencies near these roll-off points, this roll off can greatly deprecate performance if it doesn't decrease at a large enough rate. With CTLE, a tradeoff is made where in lower frequency spectral content is lowered in order in order to boost the content near the Nyquist frequency, and push higher frequency content down shown in Figure 2.5. There are two types of CTLE, passive and active, and as their names suggest, passive CTLE adds no new energy to the system while the active CTLE adds energy and as a result will have gain greater than one at some frequencies. Passive CTLE was chosen for this project for its linearity, low-cost, and ease of implementation. Passive CTLE also suffers from a few notable disadvantages; it adds no new energy to the system, and as a result the overall loss at the Nyquist frequency will be increased as well as any energy seen at all of the other harmonic frequencies.

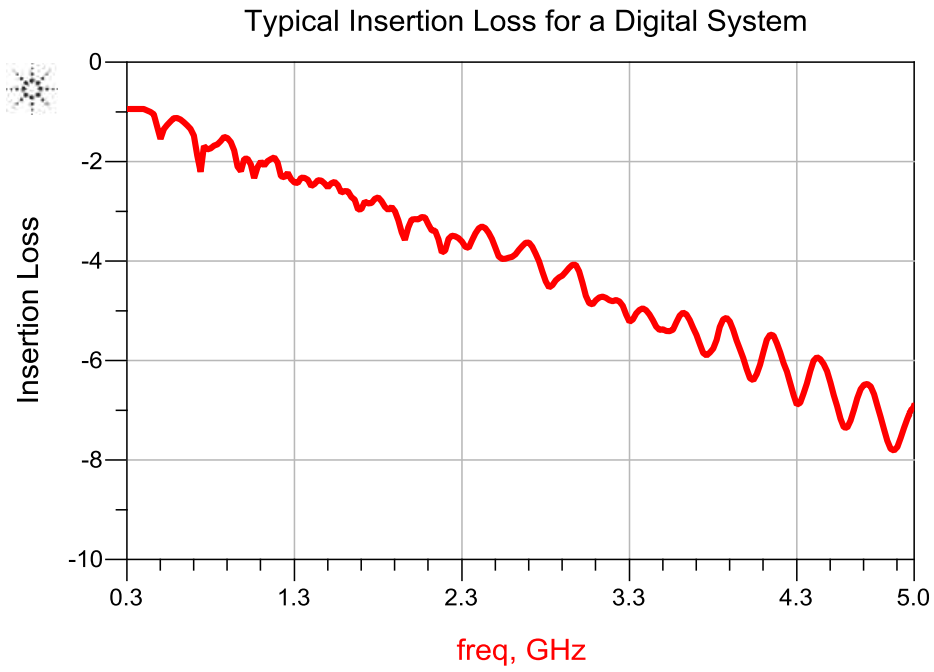

Figure 2.4 Typical channel response for a digital system

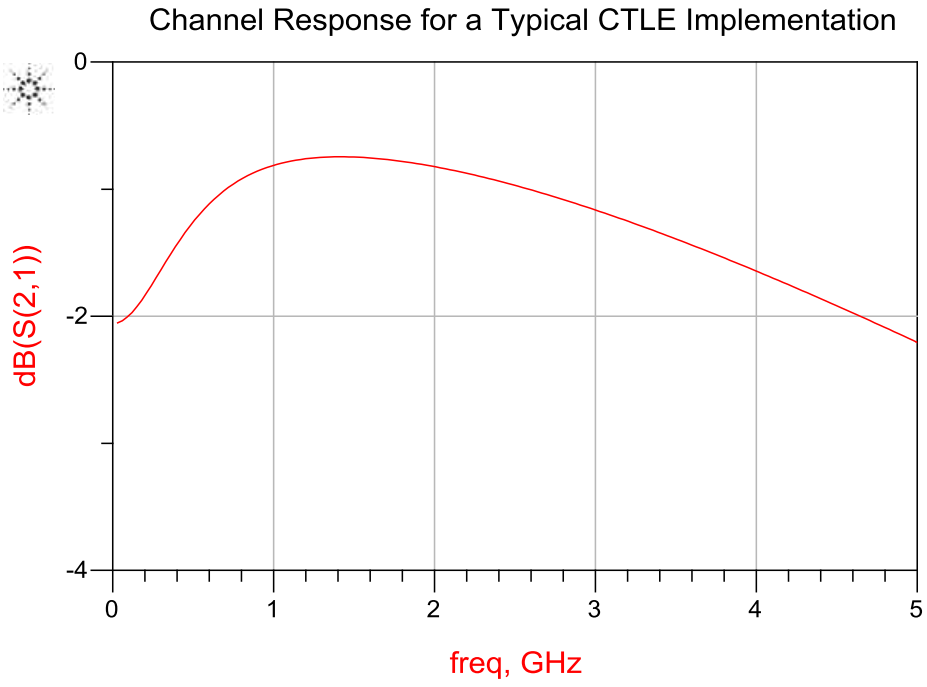

Figure 2.5 Channel Response for a CTLE Implementation

Transmitter de-emphasis was also studied, which is most conveniently thought of as an FIR (finite impulse response) filter [7]. Instead of focusing on how to improve the high frequency performance of the system, transmitter de-emphasis focuses on increasing the spectral power of the relevant frequencies in the signal transmitted. This signal can be created by taking a typical digital system and passing it through the aforementioned FIR filter. A representation of this system is found in Figure 2.6.

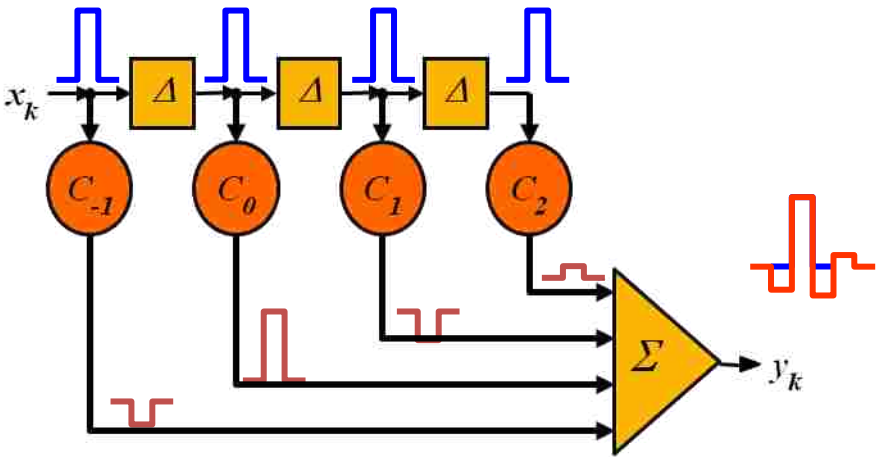

Figure 2.6 Transmitter de-emphasis system [8]

There are two types of emphasis that are used to improve performance. De-emphasis means adding no new energy to the transmitted signal, and therefore the absolute value of its filter coefficients must sum to less than one. However, in pre-emphasis, the coefficients sum can be greater than one, and some gain is added to the filter. Transmitter de-emphasis FIR filter coefficients can also be optimized to cancel pre or post cursor ISI, making it a far more generalized solution. Many of the advantages and disadvantages of transmitter de-emphasis are

shared with the CTLE: linearity; low-cost implementation; ease of implementation. Its generality also makes it challenging to tune the filter coefficients making the use of a backchannel necessary for tuning.

DFE is a fairly new method of equalization [8]. It is not typically used in many systems as it is difficult to implement and introduces non-linear effects. This technique receives a digital signal and makes a symbol decision. This decision is then passed through an FIR filter which is optimized such that post-cursor ISI caused by the last symbol sent can be subtracted from the next symbol. In Figure 2.7, a block diagram showing the many subsystems within DFE is shown. This means that the filter coefficients must be optimized for any unique channel, which makes it less general than transmitter de-emphasis, but offers a greater performance enhancement. Another benefit is that higher frequency components of a signal can be boosted but, because a symbol decision is made, the noise of the high frequency components does not get boosted. Some disadvantages, excluding the implementation costs and non-linearity already mentioned, are the inability to cancel pre-cursor ISI and the chance for error propagation caused by an incorrect symbol decision.

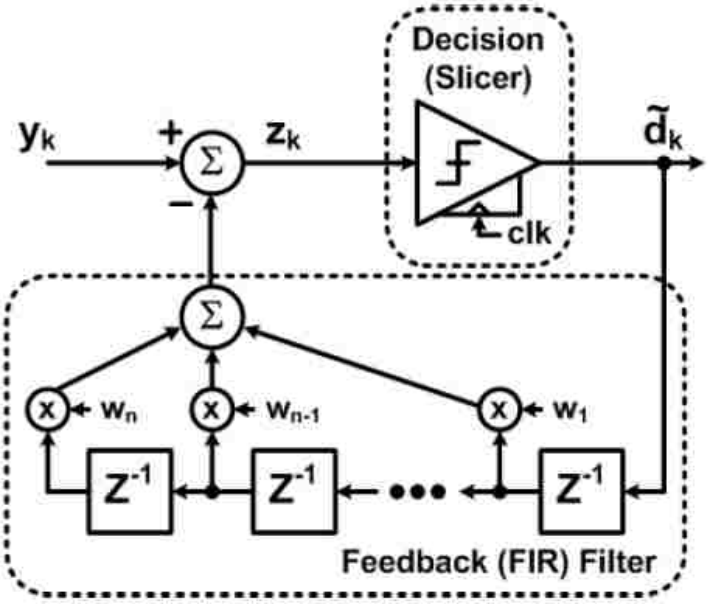

Figure 2.7 Decision feedback equalization system [8]

Each of these different signaling schemes are implemented through the use of Agilent's Advanced Design Systems (ADS) [9] component level simulator. In order to justify whether or not these design decisions have improved the overall performance of the system, eye diagrams are used to validate and analyze the effect of the different schemes. Eye diagrams are the most useful form of analysis for these signal schemes as it can be difficult to judge the effect of ISI through the use of s-parameters or TDR simulations and, as eye diagrams are greatly influenced by the input response, making them the best method to analyze ISI.

3. MEASUREMENT OF SYSTEM

This chapter will outline the measurement process overtaken for this PCB-PCB connector system. These components were measured both in the frequency and time domain, using the Time Domain Reflectometry technique for time domain, and a network analyzer for the frequency domain measurement of S-parameters. A quick explanation of these two techniques and how they are used to characterize and gain intuition about a system will be provided. Followed by a more detailed account of how this particular system was measured. Proceeded by the results and some analysis.

TDR, or time domain reflectometry, is the primary way in which an engineer can discover where elements of a system have large discontinuities. These discontinuities can effect performance in very substantial ways due to the mismatch of impedance a voltage wave, carrying a digital signal will see as it passes through a component. TDR works by inputting a voltage wave through the system and as the wave sees discontinuities, part of the wave will reflect back towards the source where it can then be measured. This voltage measurement can be post-processed to find many important features of the discontinuities including the reflection coefficients and impedances. It can also be processed to find lumped element component values by which to model a discontinuity. As well as providing insight into whether a discontinuity is behaving inductively or capacitively. In conjunction with a solid intuition about how fields in structures behave, TDR can provide a great deal of insight in how a signal travels through a component and how, when, or where its energy is being reflected.

Network analyzers are a necessary asset whenever network theory can be used in the evaluation of a system. Generally, network analyzers are used for frequency domain analysis of S-parameters but also commonly used to measure Z-parameters and smith charts. These concepts are all inter-related and are essentially different representations of the same concept: the ability

to pass current and voltage waves through a system at a particular frequency. Network analyzer theory is quite complicated, but essentially an incident voltage wave at a particular frequency is used as input to a system, the system will then reflect part of this signal back. This reflected signal will be isolated and measured. Part of this signal will pass through the system and this will also be measured. The ratios of these measured values to the incident wave are called the reflection and transmission coefficients respectively. These coefficients can be used to find the S-parameters for cases of an arbitrary number of ports and by sweeping the frequency of the input wave. It is important to note that the definition of S-parameters requires that all ports which are not being excited or measured must be terminated with the system impedance.

S-parameters can provide a great deal of information about how a system will respond at a particular frequency, which is especially important for the Nyquist frequency of a data rate. They can also be used, to a lesser extent than TDR, to find where discontinuities in a system are by converting resonant frequencies into wavelengths and seeing how these lengths correspond to the physical geometry of the components. S-parameters, as a dataset, are standardized allowing for the convenient use of S-parameter data in many different simulation softwares. This makes S-parameters the principle measurement needed when running TDR and eye diagram simulations, as well as many other simulations related to signal integrity.

For the TDR measurement of this system, a () Tdr was used [10]. This TDR has blank rise time which allows for roughly a blank spatial resolution for this model. The TDR is connected through high performance SMA coax cables to some SMA adapters to the board at one end of the board. The other side of the board was then terminated with an open load for the single ended cables and differential cables, this setup can be seen in Figure 3.1. This process was

done for all the design variations of the flex cables. Each measurement was repeated twice with two physically identical paths to test reproducibility of the measurements.

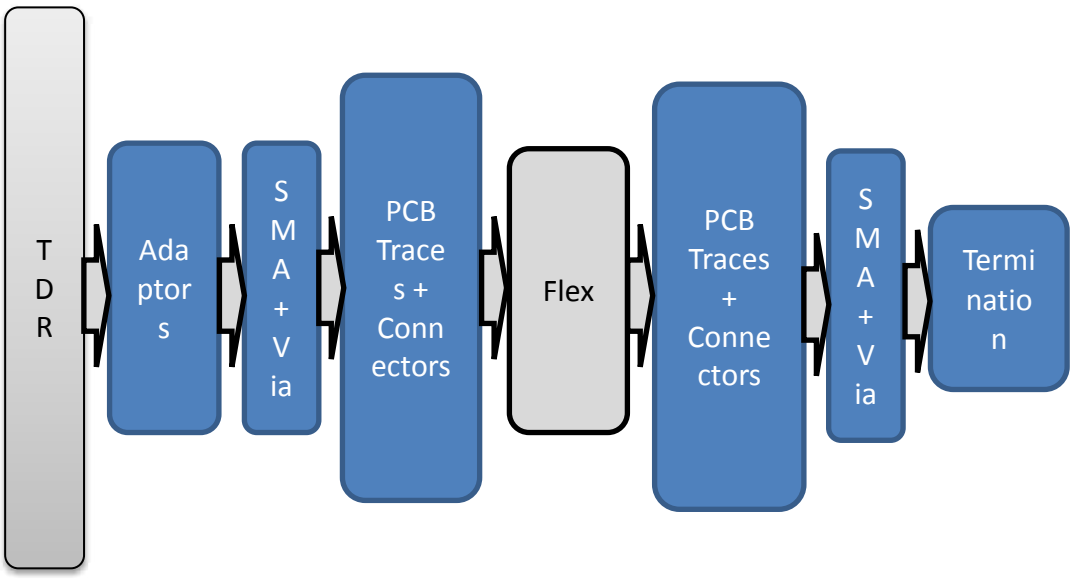

Figure 3.1 TDR measurement setup

For the S-parameter measurements, high performance cables were also used at both ends of the system. The cables also connected through the SMA adapters to the trace of the PCB board.

For the single ended cable case a de-embedding technique was used called TRL (through-reflect-line) calibration [11]. Which allowed the measurement plane to be moved very close to the PCB-flex cable connector, meaning the losses and reflections of the PCB board can effectively be ignored. TRL works by taking three separate measurements called standards: a THROUGH which is basically a trace with any length; a REFLECT which is large load termination typically implemented with an open.; a LINE which is like the THROUGH standard,

but must have the same propagation constant and impedance as the measured trace and whose electrical length must be set such that the difference between the TRHOUGH and the LINE must be between twenty and one hundred sixty degrees. With these three standards measured, an error correction model can be calculated and used to post-process the S-parameter measurements. Because the electrical length restriction of the THROUGH standard, our TRL calibration lines must include two THROUGHS, in order to get the appropriate frequency range.

TRL calibration cannot be used on a differential line, and therefore a much simpler calibration was performed at the ends of the high performance cables. This simpler calibration puts the calibration planes at the ends of the high performance SMA cables. This is a simpler approach as compared to the TRL technique, as only one measurement is taken to characterize the cable, which can then be post-processed out of the measurement. However, there is a drawback to this method which will have an impact to the simulation of the system. This measurement will include some losses from SMA adapter, causing extra losses that will be hard to account for in a model to measurement comparison.

Using the () S-parameter [12] measurements were taken up to 25GHz using a linear sweep of 1001 pts and an IFBW of 10kHz. Once again, measurements were taken for all the design variations, and using two identical paths to insure reproducibility.

In Figure 3.2 and Figure 3.3, we can see the results of the S-parameters for the single ended case. These results show the magnitude of S_{21} and S_{11} for the varying lengths of flex cable while holding the trace geometry constant (microstrip or stripline). Some patterns can be found in this data that suggests that we can trust the results. First, as the lengths of the flex cables increase the rate of loss by frequency in the |S21| is increased. This aligns with expectations as the attenuation components that dominate the |S21| are directly proportional to length. So, with

all other variables held constant, these attenuation values will increase with an increase with length and total S_{21} losses will increase. Another characteristic that leads to the confidence in the accuracy in the measurements is the fact that the stripline case has slightly larger S_{21} losses due to an increase in dielectric losses typical in a stripline geometry.

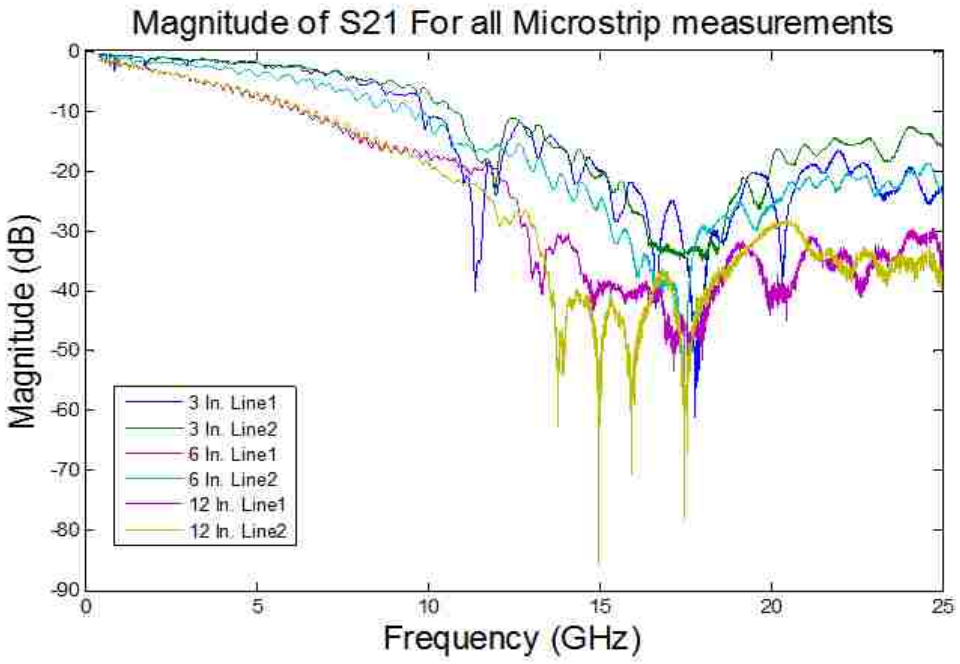

Figure 3.2 Measured S_{21} loss of microstrip cables for all lengths

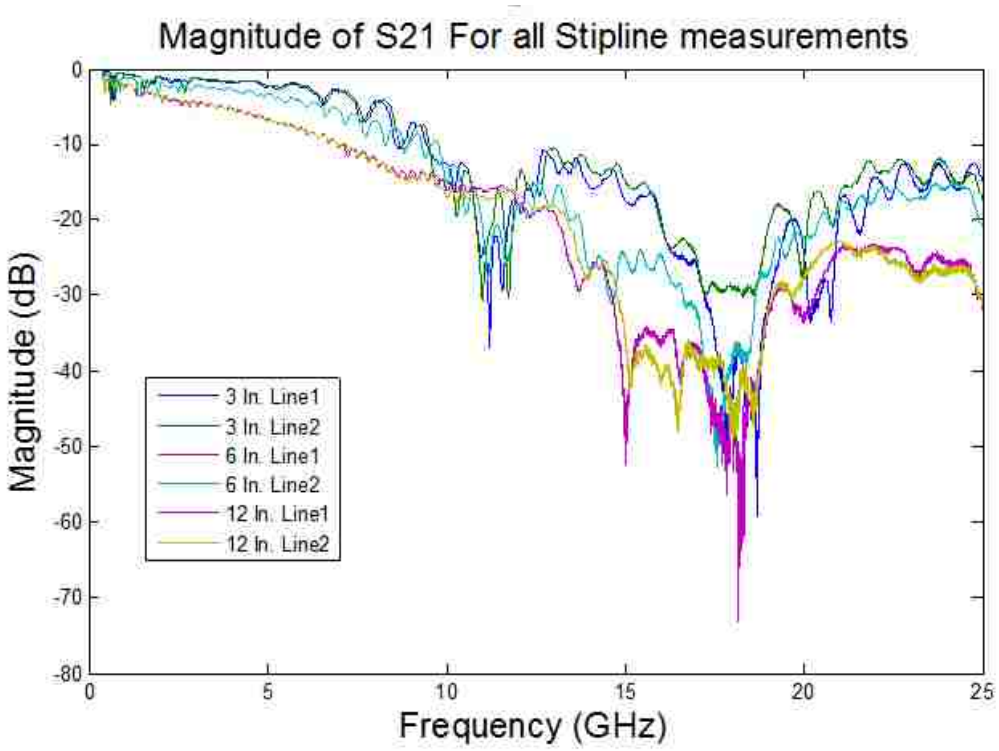

Figure 3.3 Measured S_{21} loss of stripline cables for all lengths

The length of the cables can also have a substantial effect on the S_{11} measurement. A typical characteristic of an S_{11} for a digital system is a set of rolling hills and troughs. These resonances are a result of the electrical lengths of the transmission lines within the system geometry. As these lengths increase these hills become more repetitive as the relationship between wavelength and frequency is inversely proportional. In the S_{11} results seen in Figure 3.4 and Figure 3.5, it can be seen that the hills do increase in repetition as length increases at frequencies below roughly 12 Ghz. At higher frequencies the hills occur more homogenously across the different lengths, this could be explained by large discontinuities in small geometries that are found in all three length variations. This suggests that this large discontinuity occurs in the trace to connector or the connector to trace.

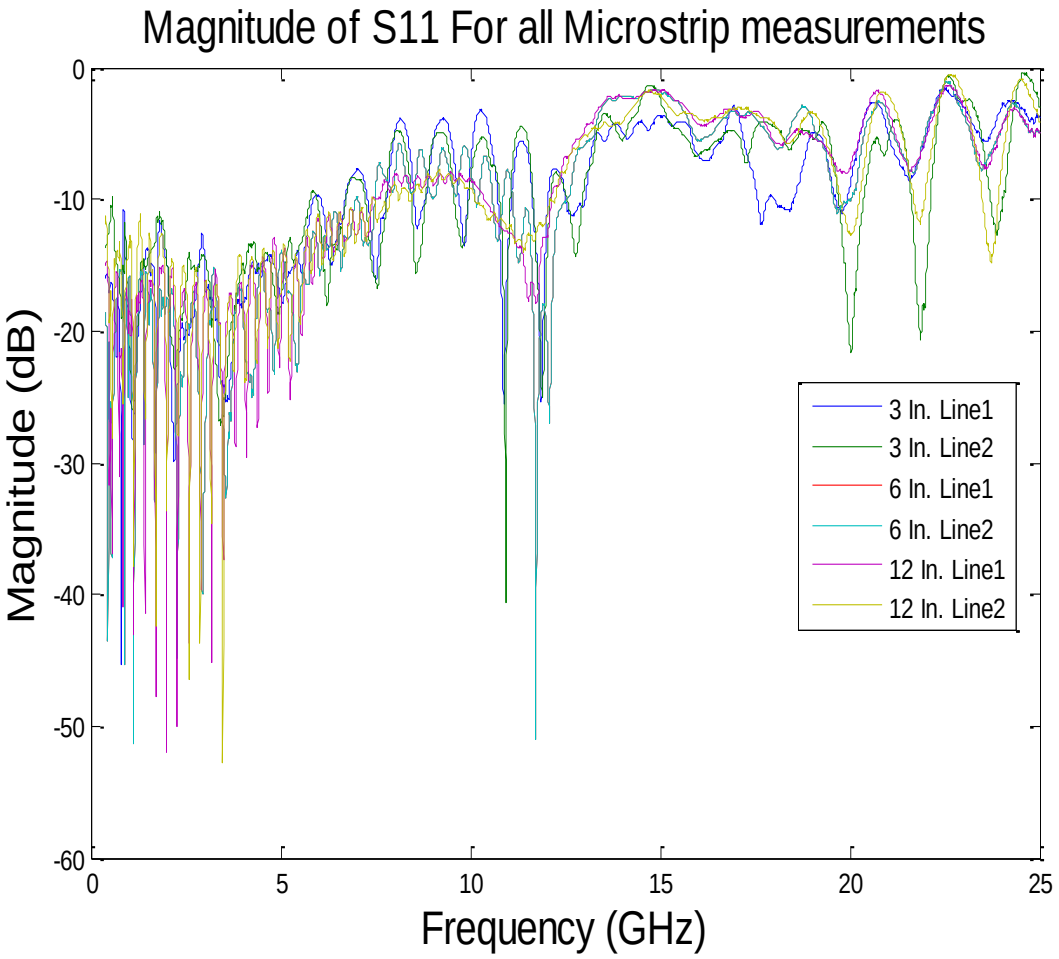

Figure 3.4 Measured return loss of microstrip cables for all lengths

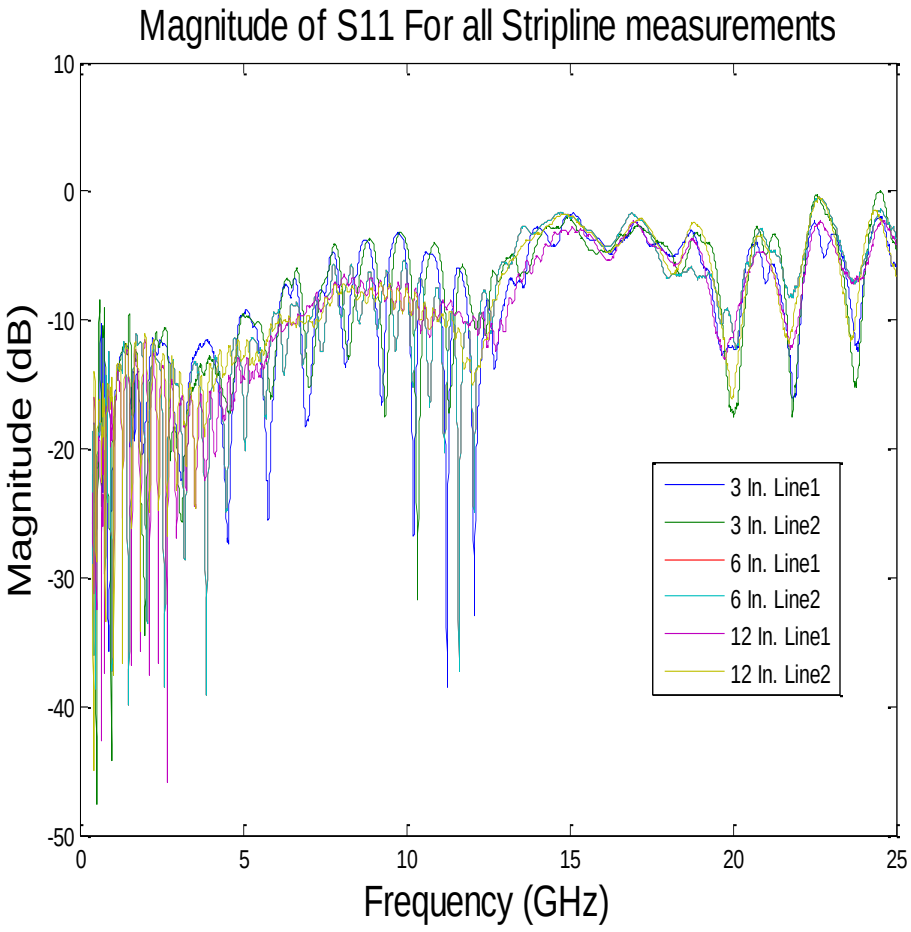

Figure 3.5 Measured return loss of stripline cables for all length

The digital performance of this cable can be estimated through the S-parameters by looking at its S_{21} losses at the Nyquist frequency. For this study, three data rates are studied three, six, and eight Gbps which have Nyquist frequencies of 1.5, 3, and 4 Ghz respectively. Oftentimes, -6 dB S_{21} loss is used as a rule of thumb to analyze loss. This rule of thumb is chosen due to the fact that -6dB is the value that an eye diagram will lose roughly half its height. For these measurements, and for the Nyquist frequencies that have been chosen to study, it can be seen that the -6dB threshold is met in nearly all cases. However, for the 12'' cables it can be seen

that the losses are fairly large at higher Nyquist frequencies which suggests that there may not be an eye opening for these higher data rate cases.

The return loss for a system is also used to predict performance. In this case the rule of thumb for the return loss is to keep the return loss below -10dB for frequencies below the Nyquist frequency. From the measurements we see that this criteria is met up to about 5 Ghz for both the microstrip and stripline geometries and for all lengths.

For the differential S-parameters, single ended four port S-parameters were measured and then later translated to the hybrid, or differential S-parameters. This is a common technique as it demonstrates the systems behavior in a way that is consistent with how the differential pairs would be used in a practical application. Differential S-parameters demonstrate the effect of inputting differential or common mode inputs on one port, and shows the differential or common mode response for any port. For digital applications there is a tendency to use the S_{DD21} and S_{DD11} results, which are both differential excitations and responses expect one is the transmitted differential response while the other is the reflected differential response, respectively. Sometimes, differential to common mode S-parameters are used as these can give insight into how much the differential mode is converted to common mode noise. In this case the differential insertion and return loss will only be inspected.

The S_{DD21} loss for the both the microstrip and stripline geometries is shown below in Figure 3.6 and Figure 3.7, organized by cable length and the differential line used to make the measurement. It can be seen that the two differential lines have consistent results across the varying lengths, meaning the measurement is behaving consistently. Losses are increasing with frequency which is expected as the dielectric and conductor losses increase with an increase in frequency. There are rather large nulls in the stripline measurements at roughly 14GHz, 15GHz,

and 17GHz for the 3, 6, and 12 inch lines respectively. This change in frequency as a function of cable length suggests is caused by the connector to cable discontinuity. The microstrip does not have these sharp nulls, which could suggest that is has a better matching to the connector. One unusual aspect of these results is that the stripline geometry is about as lossy as the microstrip, which typically is less lossy due to a lower effective dielectric constant. However, in this case, a plastic layer must be placed above the conductor of the microstrip to add mechanical support. This plastic will introduce more dielectric losses for the microstrip case. In general, the S_{DD21} suggests that we can push the data rate to about 8Gbps, 7Gbps, 5Gbps for the 3, 6, and 12 inch lines respectively using the -6dB loss metric.

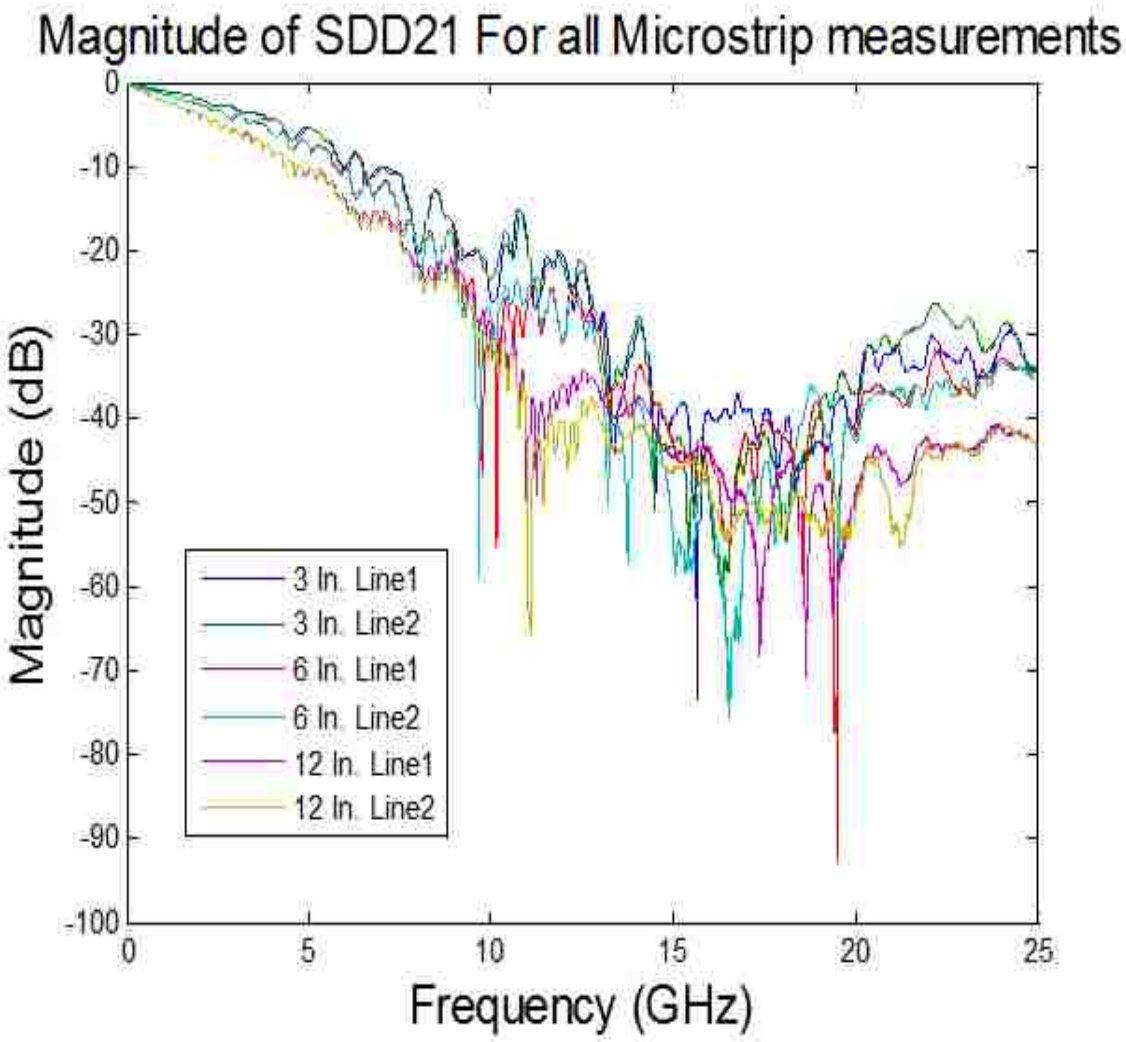

Figure 3.6 Measured differential |S21| of microstrip cables for all lengths

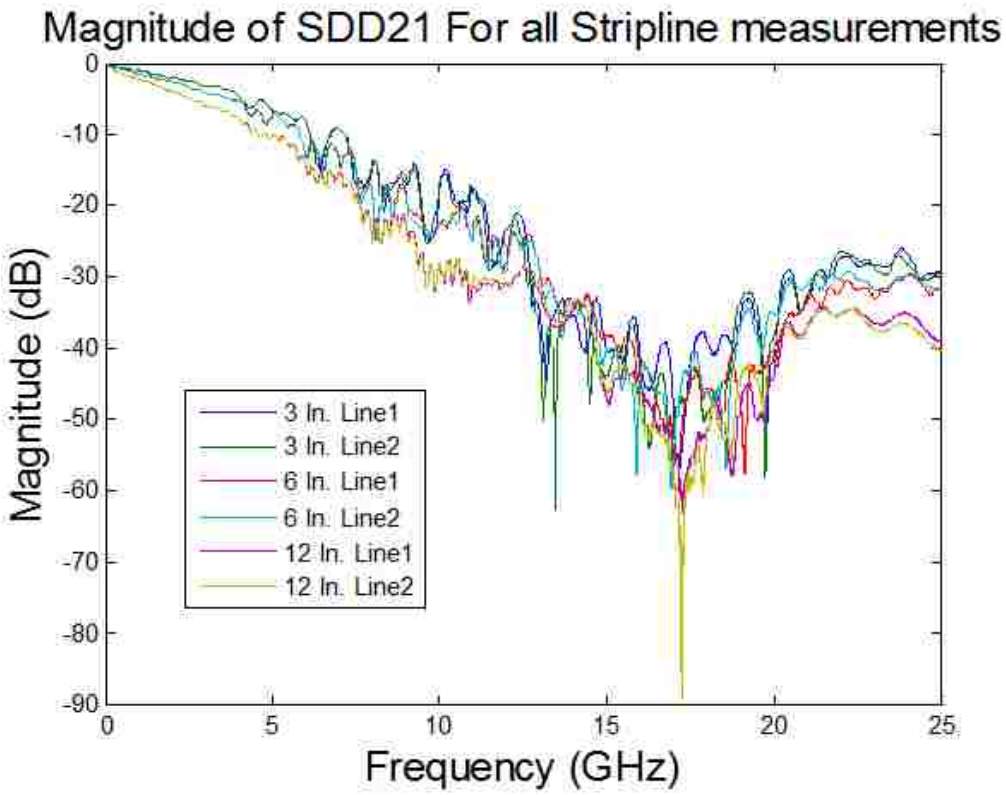

Figure 3.7 Measured differential |S21| of stripline cables for all lengths

The S_{DD11} results have a very similar analysis to the single-ended S_{11}. In Figure 3.8 and Figure 3.9 large humps can be seen in the S_{DD11} that match up across all lengths, suggesting these humps are a function of the connector discontinuities. It can also be seen that there are several smaller bumps that occur more regularly as the length of the cable increases, which is indicative of the connector to cable transition. In generally, the microstrip and stripline cables have a fairly good differential match even at higher frequencies using the -10dB metric.

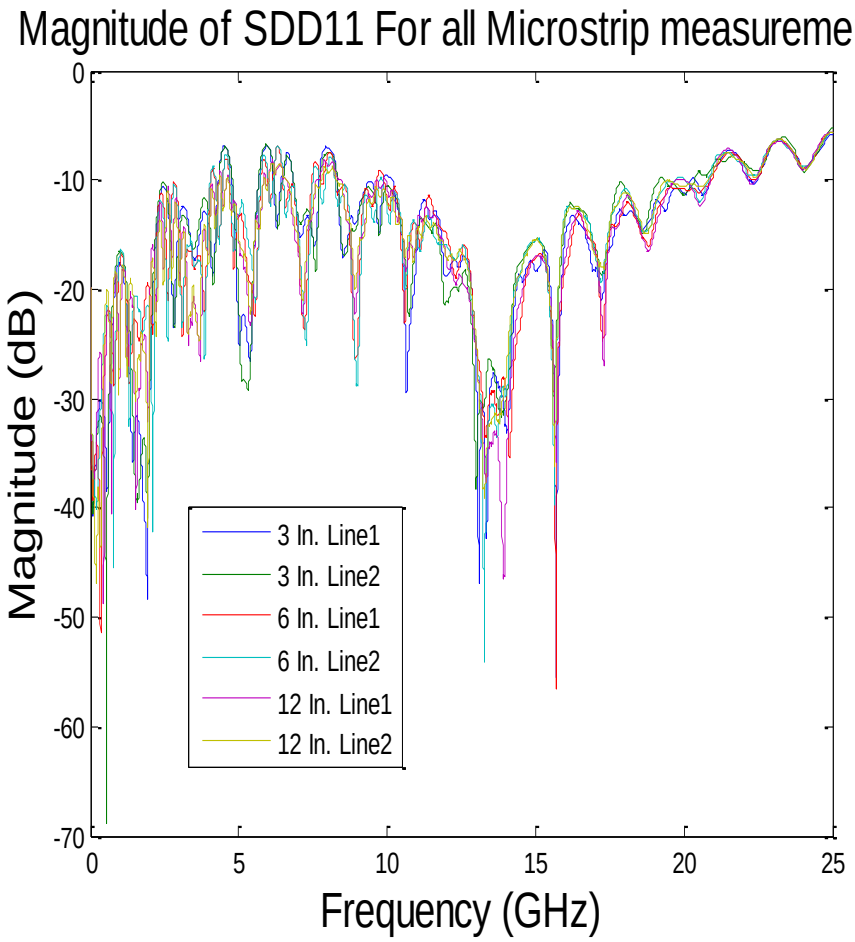

Figure 3.8 Measured differential return loss of microstrip cables for all lengths

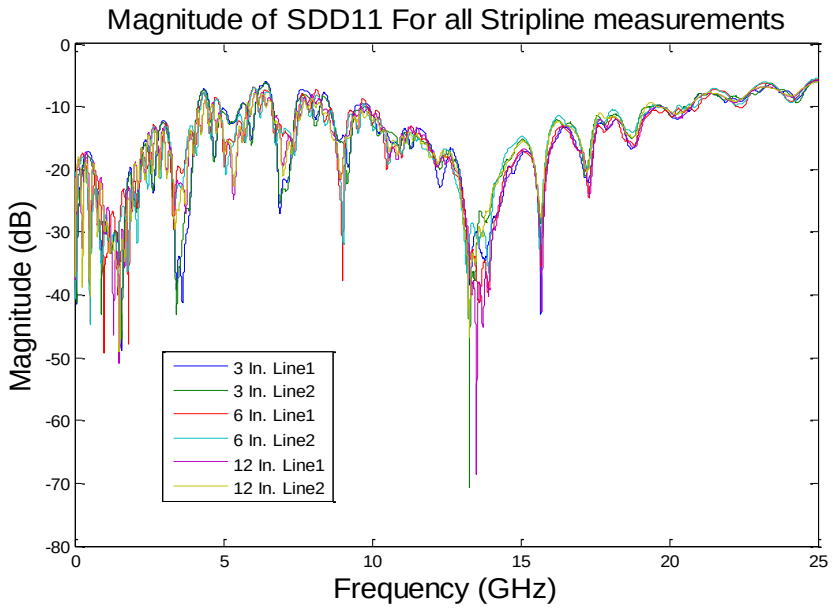

Figure 3.9 Measured differential return loss of stripline cables for all lengths

The discussion now turns to the differential and single ended TDR measurement results. In the Figure 3.10 and Figure 3.11 shown below the results for the single ended TDR measurements of impedance vs. time for the microstrip and stripline with each of the varying lengths. Several large discontinuities can be seen in the measurement. These discontinuities, listed chronologically, are the SMA adapter followed by the flex cable adapter, and finally by the second flex cable adapter. As the cable gets longer, the amount of time between the two flex cable connectors increases due to increased propagation time for the increasing lengths of cable. These measurements also show what the impedance of different design variations for the cable will be. For the microstrip case, these cables have impedances of roughly 65ohms. Ideally, this cable should have an impedance of 50ohms for the best possible match, however a 10 percent margin of error is typically considered reasonable. This 65ohm cable however doesn't meet this requirement either, and may need to be redesigned in the future. The stripline cables have a much

better match, from the TDR measurement it be seen to be roughly 55ohms for all three lengths falling well within the nominal range. For the flex cables, there can also be seen some rippling in the TDR measurement which swings about 2 ohms total difference. This rippling is somewhat unusual, but could be explained by manufacturing variations in the dielectric thicknesses.

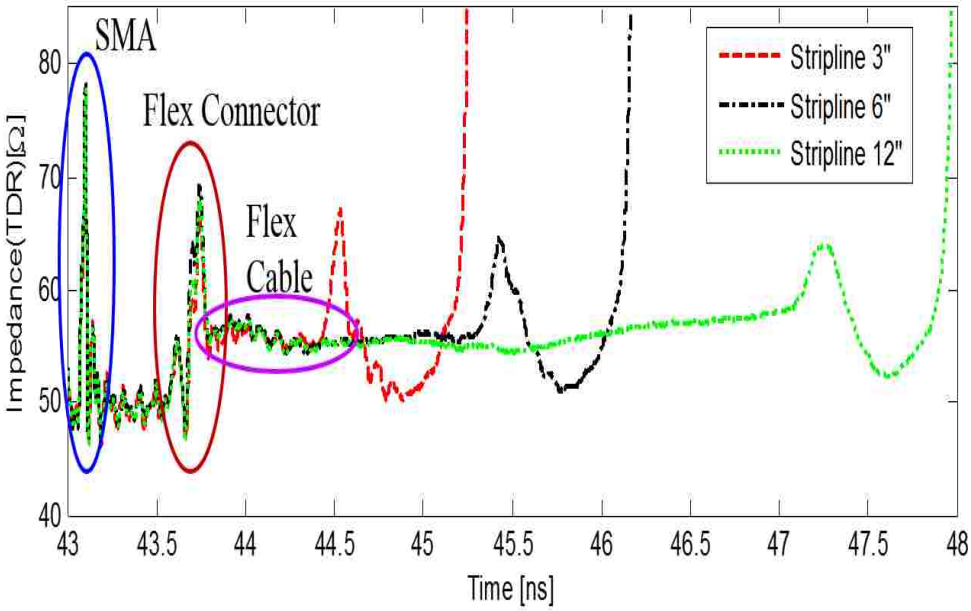

Figure 3.10 TDR measurement results of stripline cables for all lengths

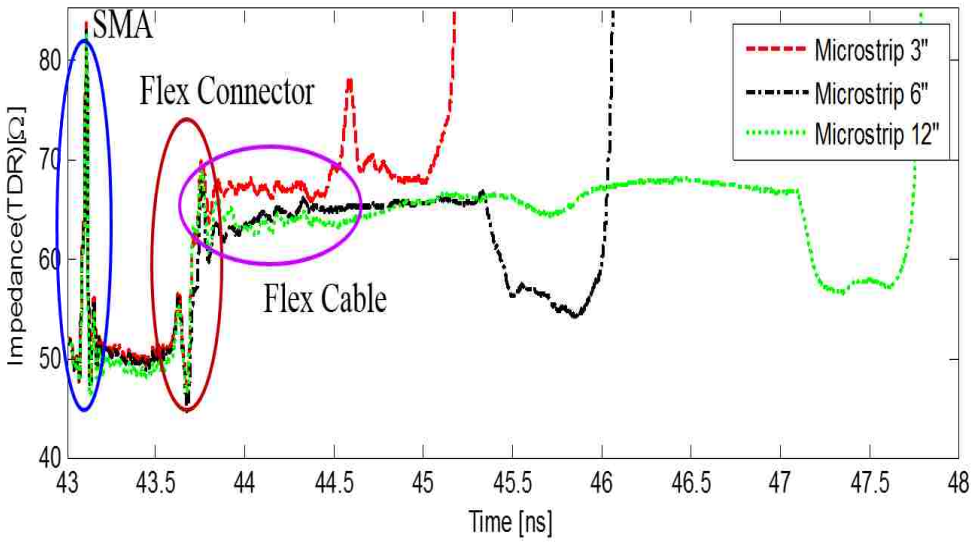

Figure 3.11 TDR measurement results of microstrip cables for all lengths

The differential TDR measurements are fairly similar with respect to the single ended measurements, as seen by Figure 3.12 and Figure 3.13. Discontinuities are found once again for the SMA adapter, followed by the connector. In the differential case however, we see that the flex cable connector impedance dips low rather than high. This may suggest that the pitch for this connector is slightly larger than what may be needed to properly couple a differential line. Once again, the total propagation time between the two flex connectors increases as the lengths of the cables increases. For the differential case, the microstrip line has a very good flat differential impedance of 100 ohms, making this a fairly good design. However, for the stripline design, the impedance is about 85 or 90 ohms. If the same plus or minus 10 percent rule is applied then this is very nearly acceptable. However, it would probably best be redesigned if it is intended to be used in a 100 ohm differential system.

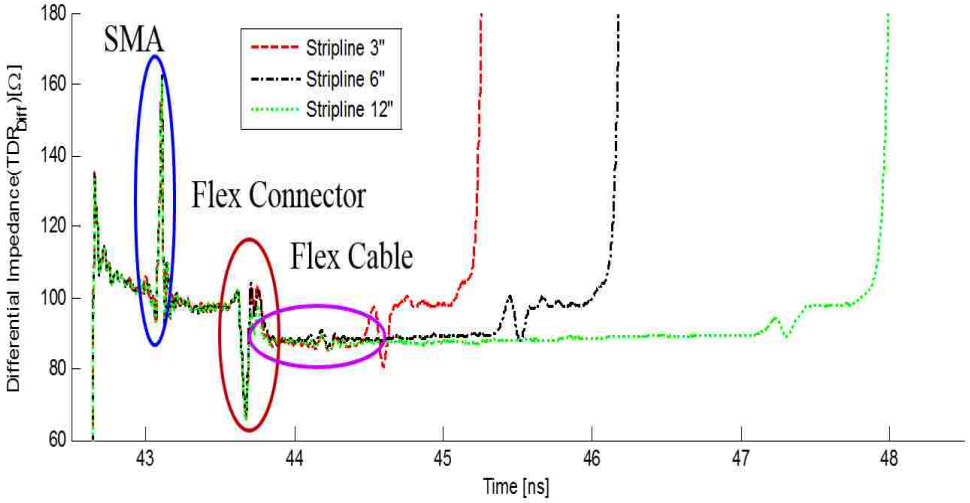

Figure 3.12 Differential TDR measurement results of stripline cables for all lengths

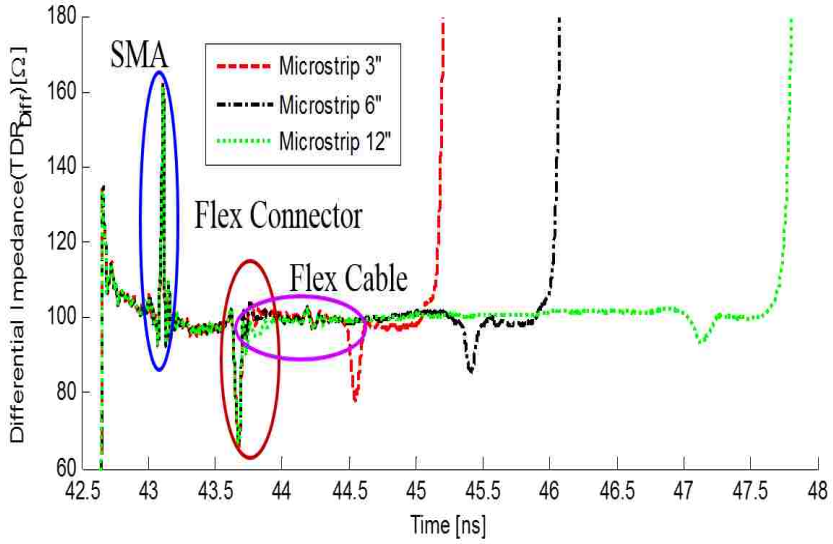

Figure 3.13 Differential TDR measurement results of microstrip cables for all lengths

4. SIMULATION OF SYSTEM

This section will continue working through the various stages of analysis. For the simulation stage, the simulator types will be briefly explained followed by the simulation setup. Finally, the results will be shown and compared to the measured values of the system.

As previously mentioned, this system requires the use of two simulator types. One of which is 3d full wave modeler. There are many different types of full wave 3D modelers using an array of different solver techniques such as FDTD. For this work, CST's transient solver was used. This solver was chosen as it allows for the construction of complicated structures, leading to a greater level of accuracy at higher frequencies. These 3D solvers however do come with their complications. Their ability to handle arbitrary geometries also increases the total simulation time as all electromagnetic fields in the solution space must be simulated. It can also be a complicated and time consuming task to create highly accurate models, especially as the wavelengths of the simulated fields become smaller and small perturbations in the geometries of the real world structures start to have an effect.

Another simulation tool used for the modeling of this system is the FEMAS arbitrary transmission line tool. This tool handles arbitrary 2D cross-sections and treats them as uniform transmission lines. This tool was used as it can quickly calculate S-parameters for very long transmission lines, thus saving the calculation time that a 3d solver would need. The primary drawback for this type of simulation tool is its inability to handle more abstract physical structures. Due to the fact that this simulator was used for the simulation of a simple transmission line, this is not a problem for this project.

For this system, S-parameters are calculated for the PCB - Connector – Cable element using the full-wave transient solver. This system has some symmetry, so simulations for this subsystem provides two subsystems worth of S-parameters, with the caveat that the ports must

be reversed for the S-parameters of one of the subsystems. Most of the cable's geometry can be modeled efficiently using the cross-sectional analysis tool, and its S-parameters can be exported. With all the subsystems' S-parameters available, a simple cascading can be done to mimic the effects of the entire system.

In order for this model to be realistic, accurate S-parameters must be extracted from the models. In the case of the 3D modeling effort, the PCB sub-element was modeled based upon the dimensions found in its design file. For the single ended cases, the board should be shortened to most accurately represent the measured data as a TRL calibration plane was used to mitigate the effects of the PCB trace. This reference plane position is also documented in the design file as are accurate dimensions for the remaining trace and connector launching pad. The material for the PCB was assumed to be FR4 with a fairly high dielectric constant of 4.1. It was also assumed that tangent delta for the FR4 was at least .02 at 1GHz. These values were chosen as they are common values for FR4. All trace dimensions this microstrip can be found on fig 1.

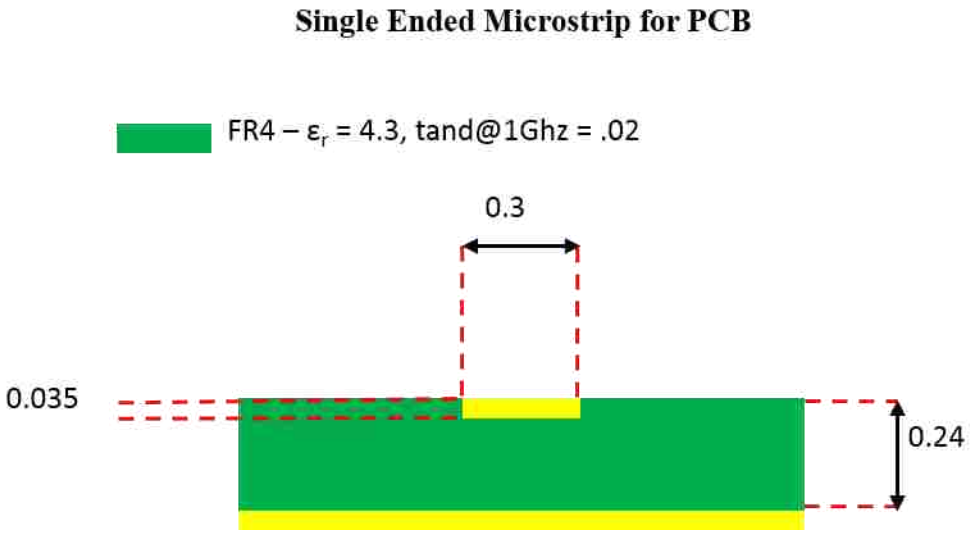

Figure 4.1 Single ended microstrip PCB geometry and material details

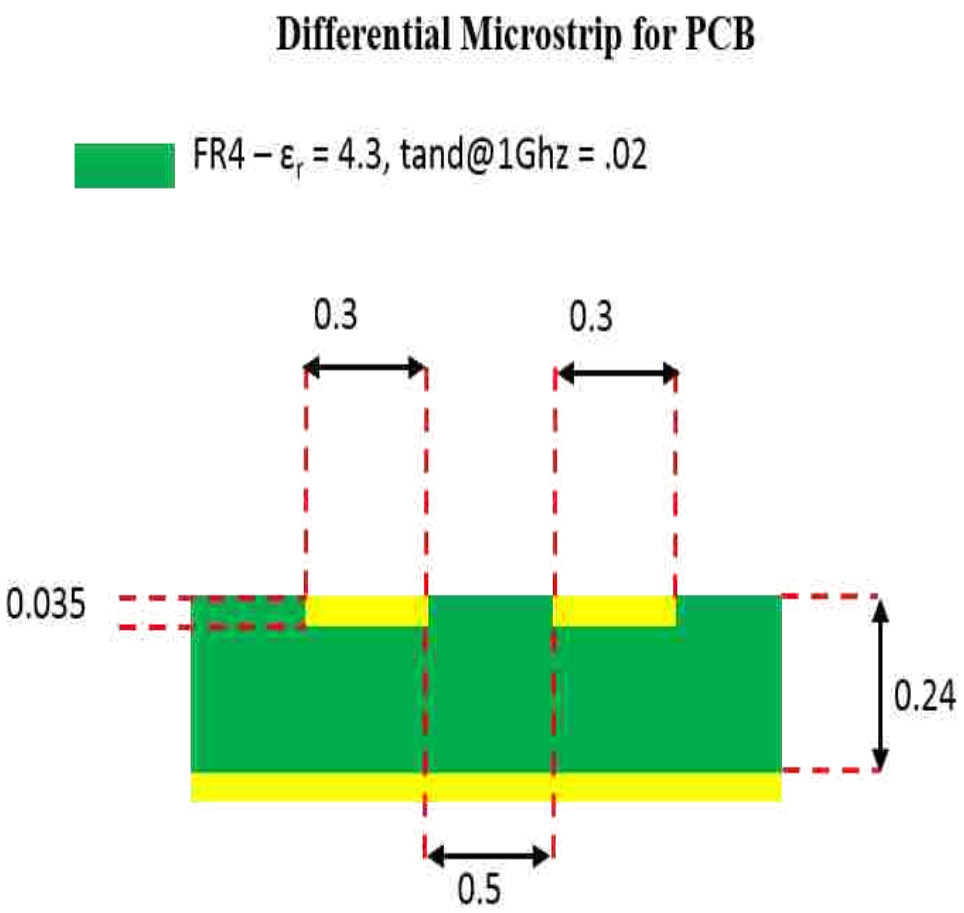

Figure 4.2 Differential microstrip PCB geometry and material details

Fortunately, a vendor model was found for the Hirose connector used in these simulations [13]. Vendor models can be very convenient when available; they can provide a highly detailed and highly accurate construction of the physical elements of a component without the large time investments of constructing a similarly detailed model. Unfortunately, the supplied model wasn't constructed for use in electrical simulators and the file types available to download caused some information loss while translating the file into the 3D modeler. This information loss was minimal, but some assumptions about the connector geometry needed to be made, slightly

reducing its accuracy. The electrical properties of the connector were assumed to have the conductivity of aluminum and a dielectric constant of polyester, which is 3.5 of with a loss tangent of .03 at 1 Ghz. Aluminum conductivity was found in a Hirose connector datasheet, while the polyester was assumed as it is a plastic typically used for low cost connectors.

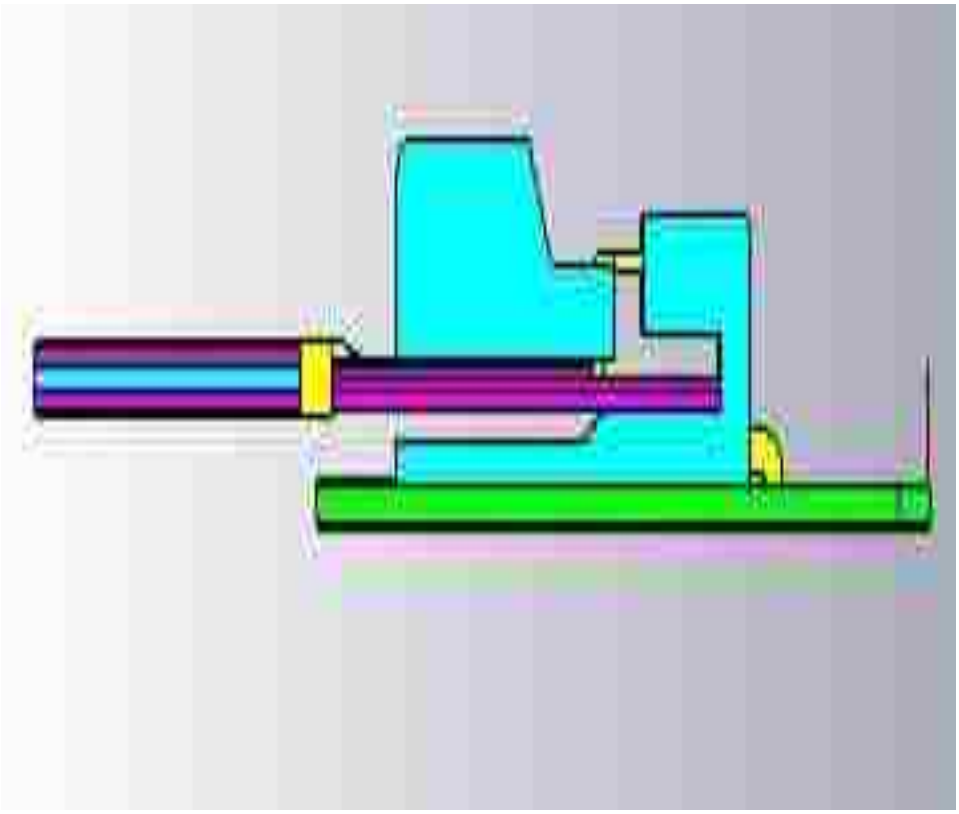

Figure 4.3 Sideview of full wave model of PCB to cable subsystem

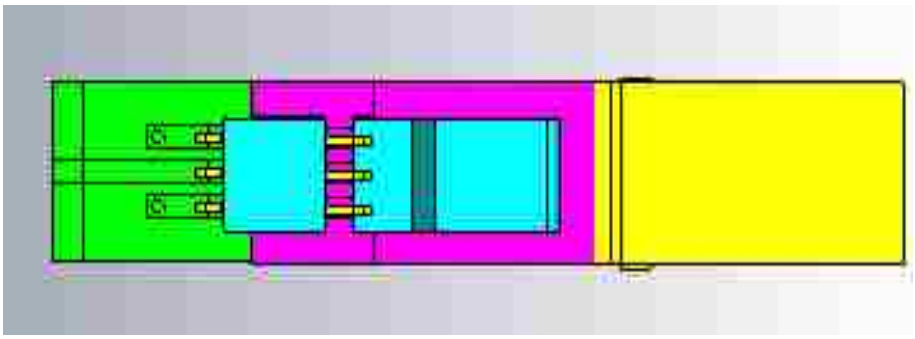

Figure 4.4 Top-down view of full wave model of single ended PCB to cable subsystem

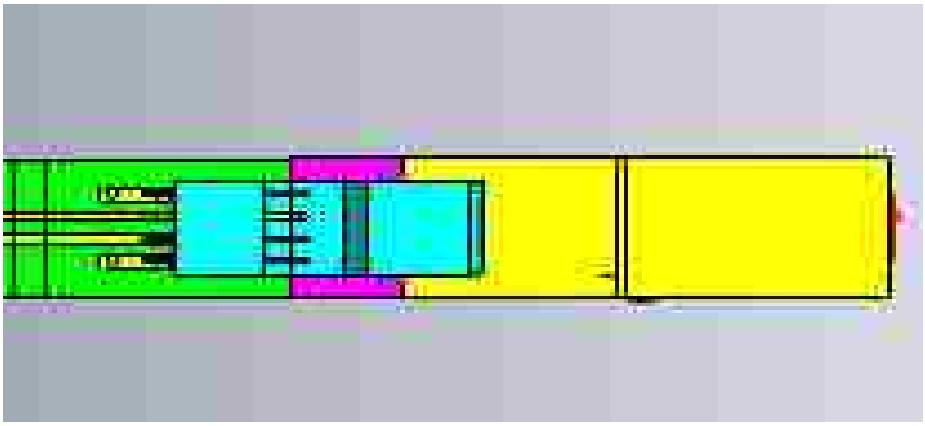

Figure 4.5 Top-down view of full wave model of differential PCB to cable subsystem

Next, the flex cable was modeled. This model was constructed by using the dimensions found in the Nicomatic design specifications, which are not publicly available. This design specification contained all necessary information about the construction of the flex cable model; including the cross-section of the many different signaling and trace geometries. Due to the manufacturing process of the cable, three dielectric layers are used in the cross-section, one adhesive layer and two polyester layers, whose dielectric and loss tangents can found to be 3.1 and 3.5 and .03 at 1GHz, with the conductors all made of aluminum.S

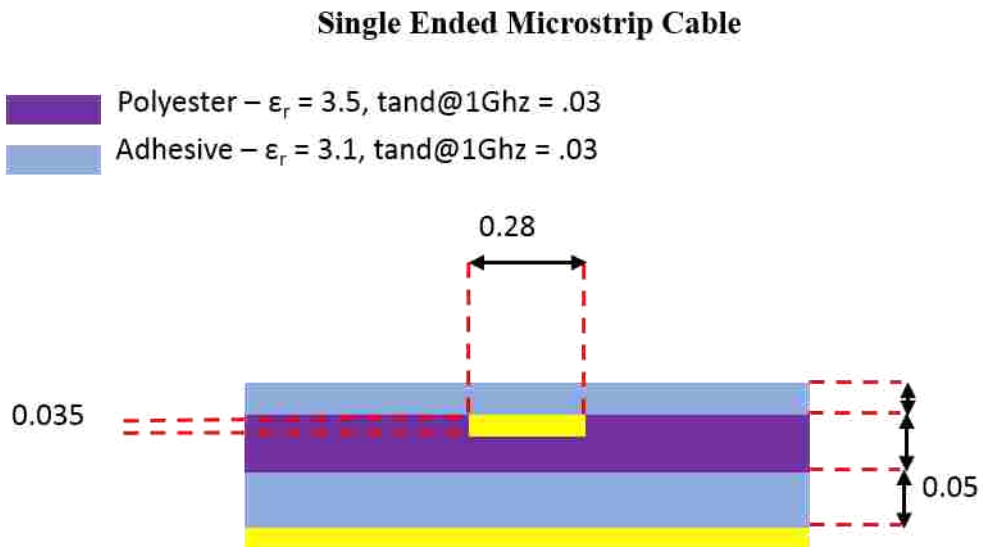

Figure 4.6 Cross-sectional geometry for single ended microstip cable in millimeters for all lengths

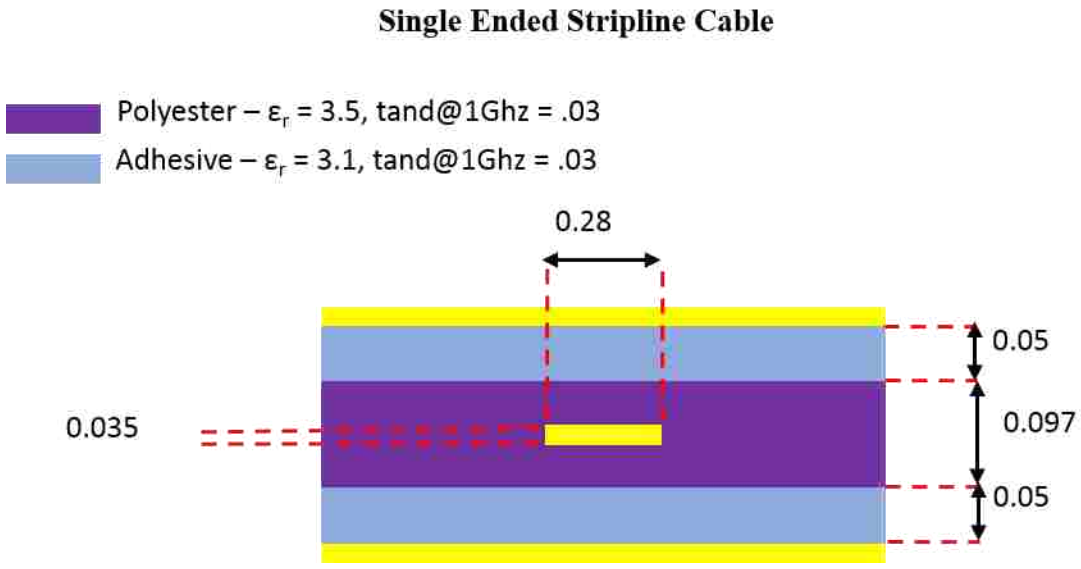

Figure 4.7 Cross-sectional geometry for single ended stripline cable in millimeters for all lengths

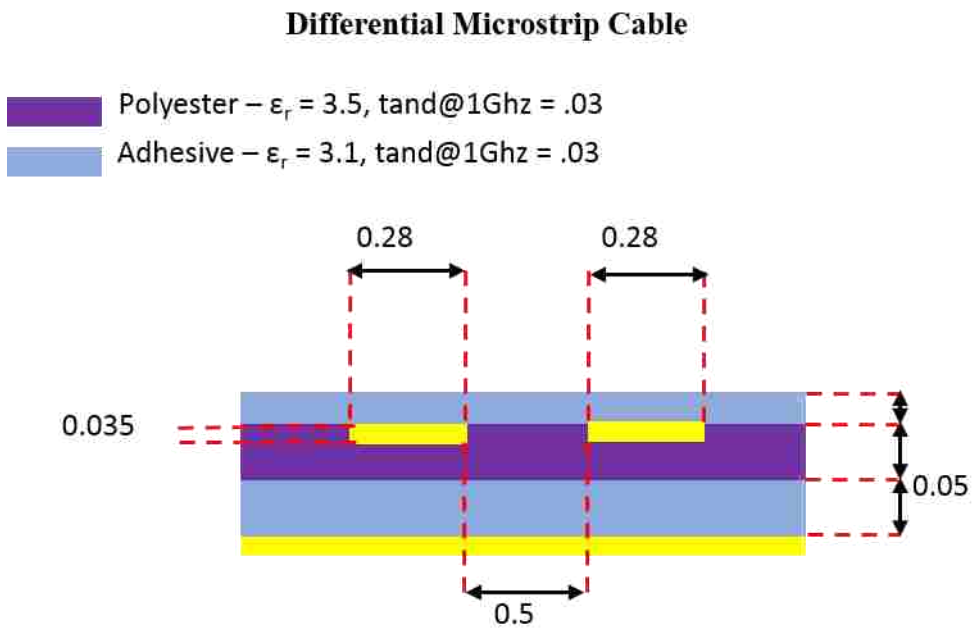

Figure 4.8 Cross-sectional geometry for differential microstip cable in millimeters for all lengths

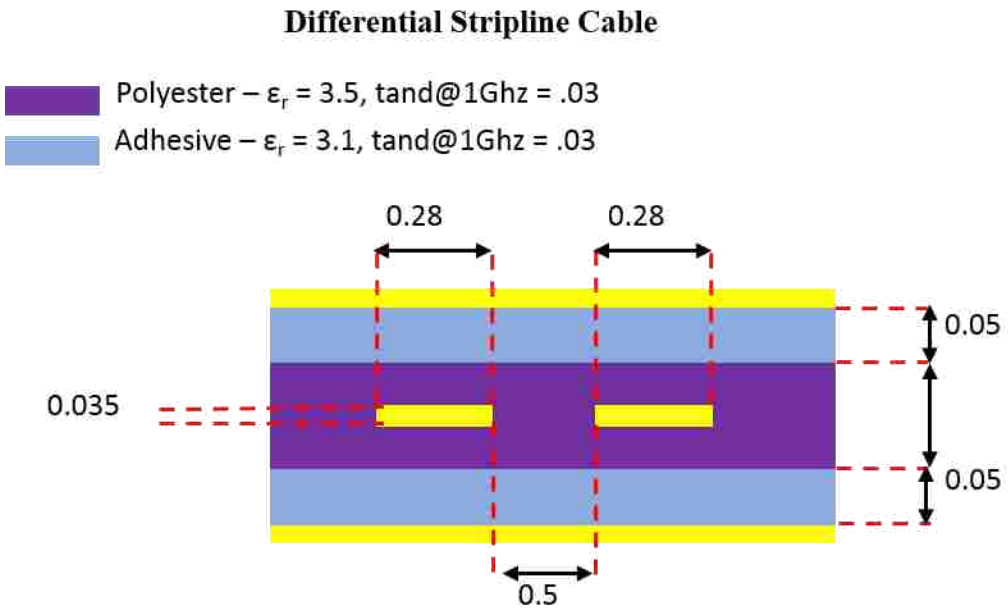

Figure 4.9 Cross-sectional geometry for differential stripline cable in millimeters for all lengths

For the transmission line modeling, only the cross-sectional geometry of the cable is needed. And as the material properties are also known, this can be thought of as an extension of the transmission line discussed in the full-wave modeling.

For each of the subsystem, S-parameters were calculated up to 10 GHz using a linear sweep of 1001 points. Ten Ghz was chosen because accurate results can be simulated in this band.

Below are the end results of this modeling effort as a comparison of S-parameters. For the single-ended case a fairly good match is made between the across the different lengths.

For the stripline case, a very good match of phase and return loss is seen for all three of the different length cables for |S21|, shown in Figure 4.1-6. For S_{11}, it is difficult to get a very strong correlation. But typically, it would be considered a good match as long as the troughs line up reasonably well which is true for this case. The phase for all cables matches very well as can be seen.

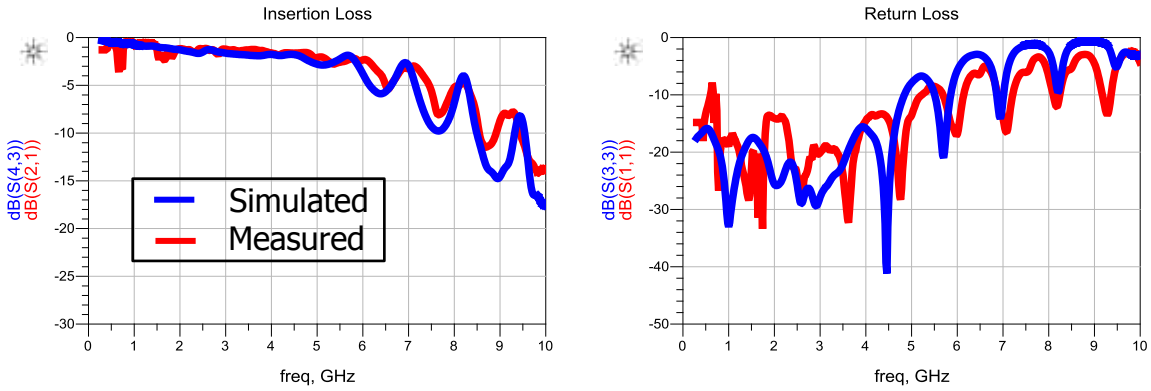

Figure 4.10 Three inch stripline correlation of measurement and simulation using S-parameters

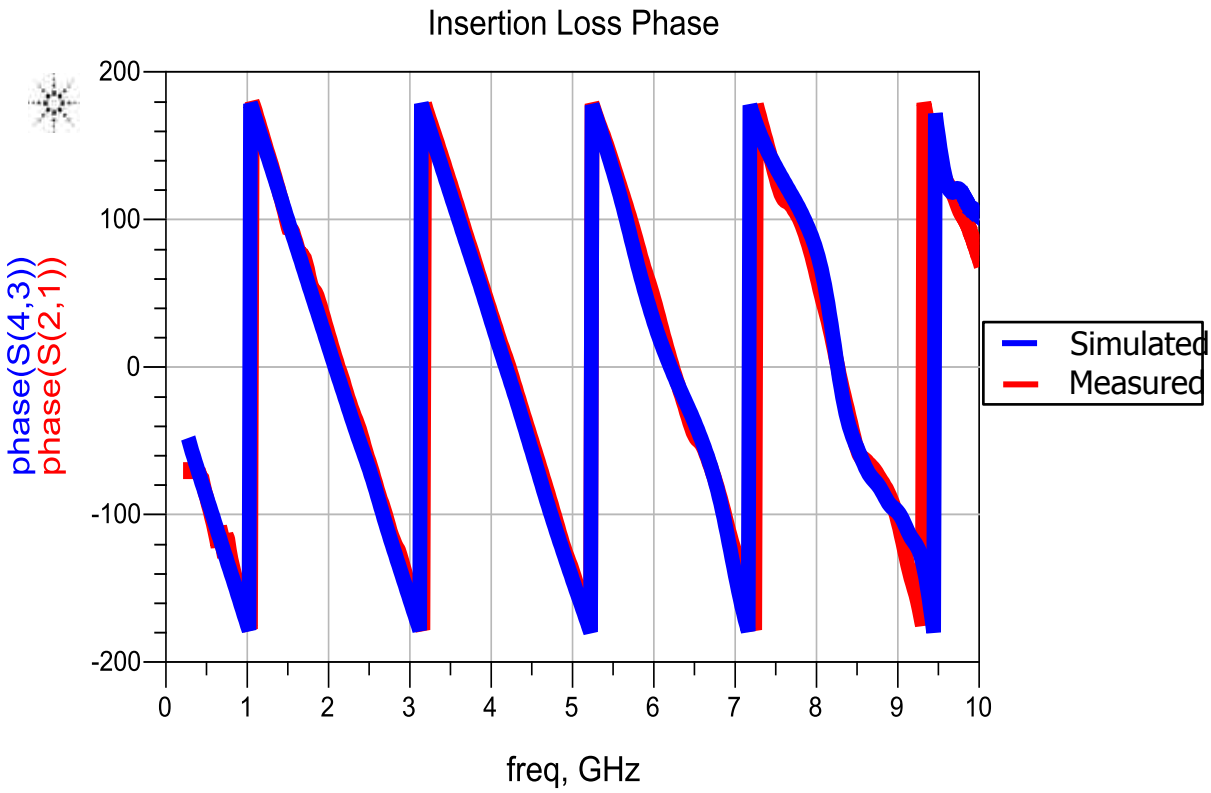

Figure 4.11 Three inch stripline correlation of measurement and simulation using S_{21} phase

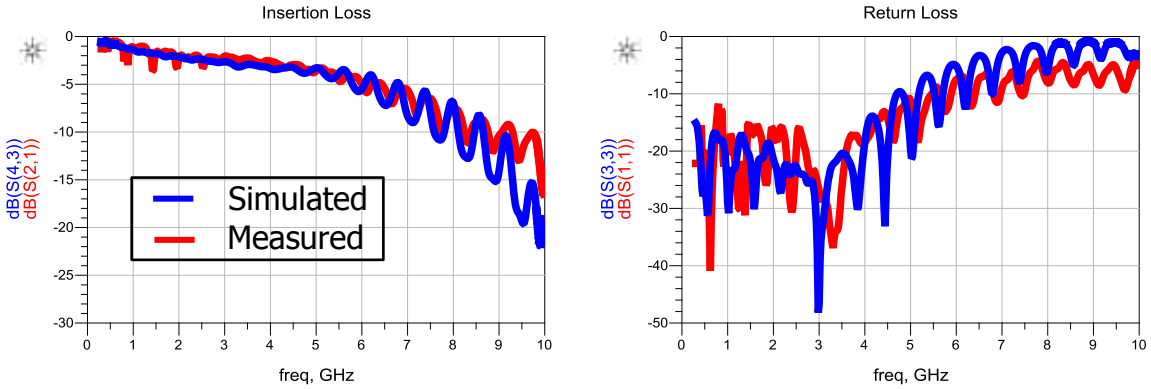

Figure 4.12 Six inch stripline correlation of measurement and simulation using S-parameters

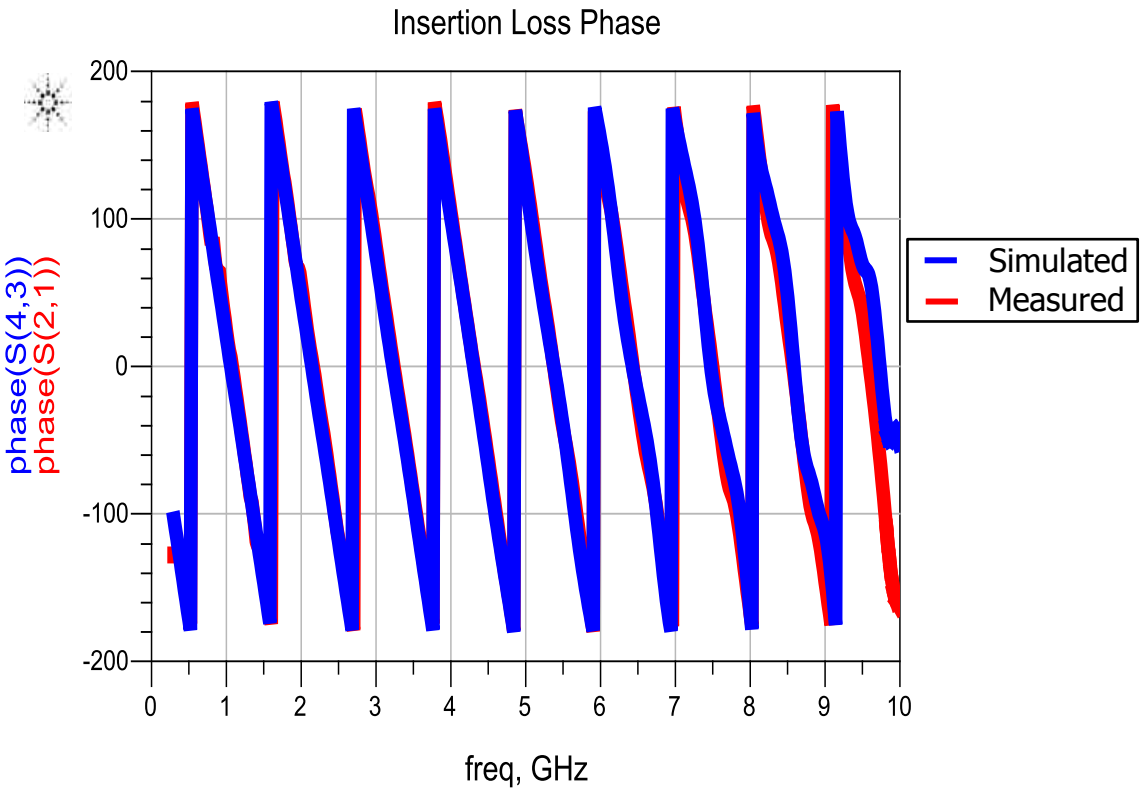

Figure 4.13 Six inch stripline correlation of measurement and simulation using S_{21} phase

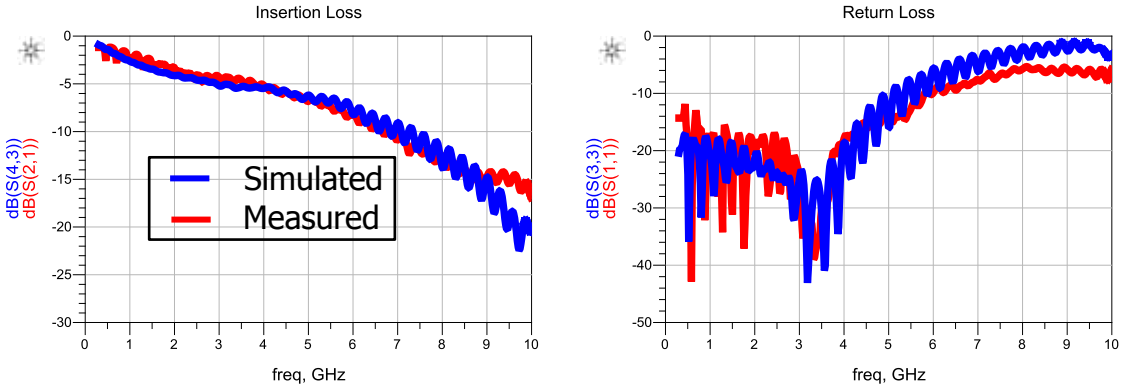

Figure 4.14 Twelve inch stripline correlation of measurement and simulation using S-parameters

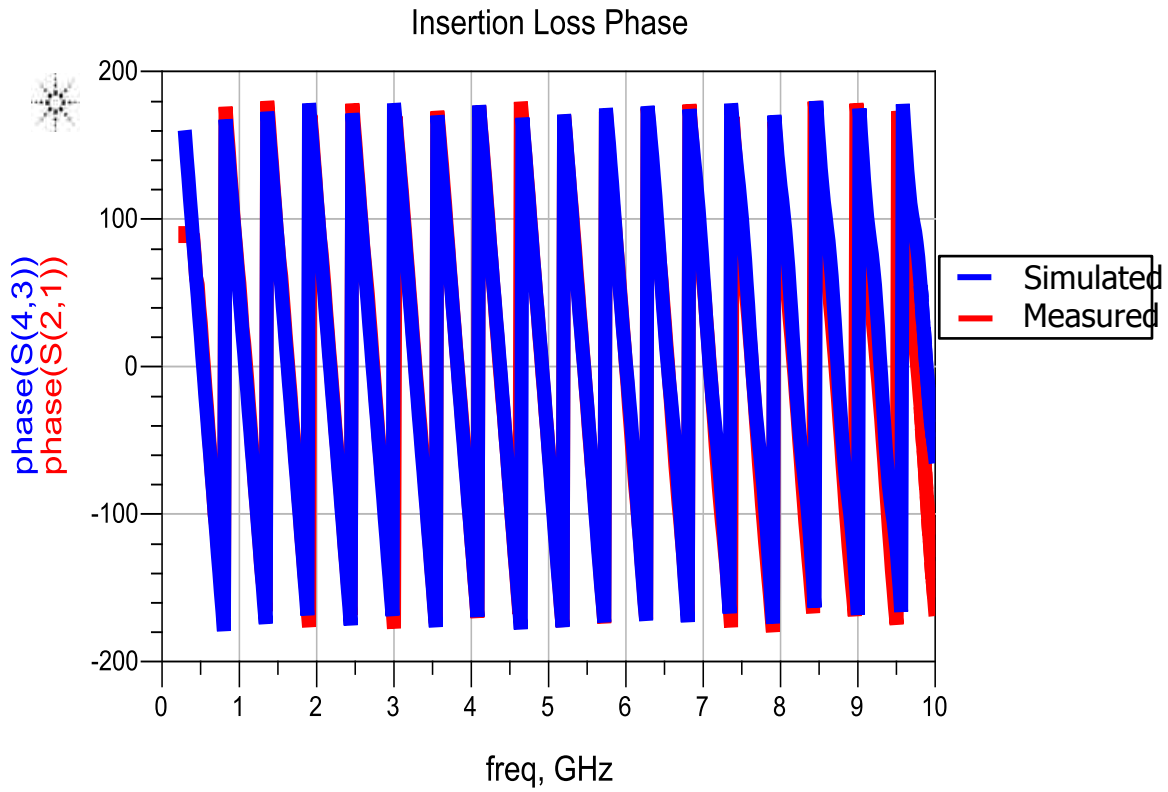

Figure 4.15 Twelve inch stripline correlation comparison of phase

For the microstrip geometry, shown in Figure 4.7-12, the results are less correlated. Especially as the case as the cables length is increased. This may be due to inaccurate geometry for the microstrip cable, which will give the wrong impedance and as a results, will produce more reflections than what may exist in reality. This is suspected do to the dips seen at higher frequencies for the microstrip case in the S_{21} magnitude losses. These dips are typically found whenever the reference impedance does not match well to the impedance seen in a geometry. Although, the correlation becomes worse at higher frequencies, lower frequency data seems to match fairly well, especially below 5 Ghz.

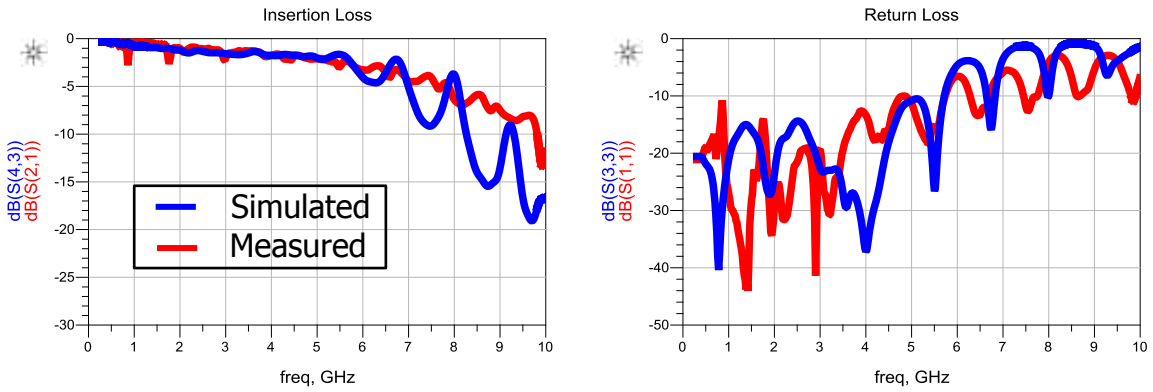

Figure 4.16 Three inch microstrip correlation of measurement to simulation using S-parameters

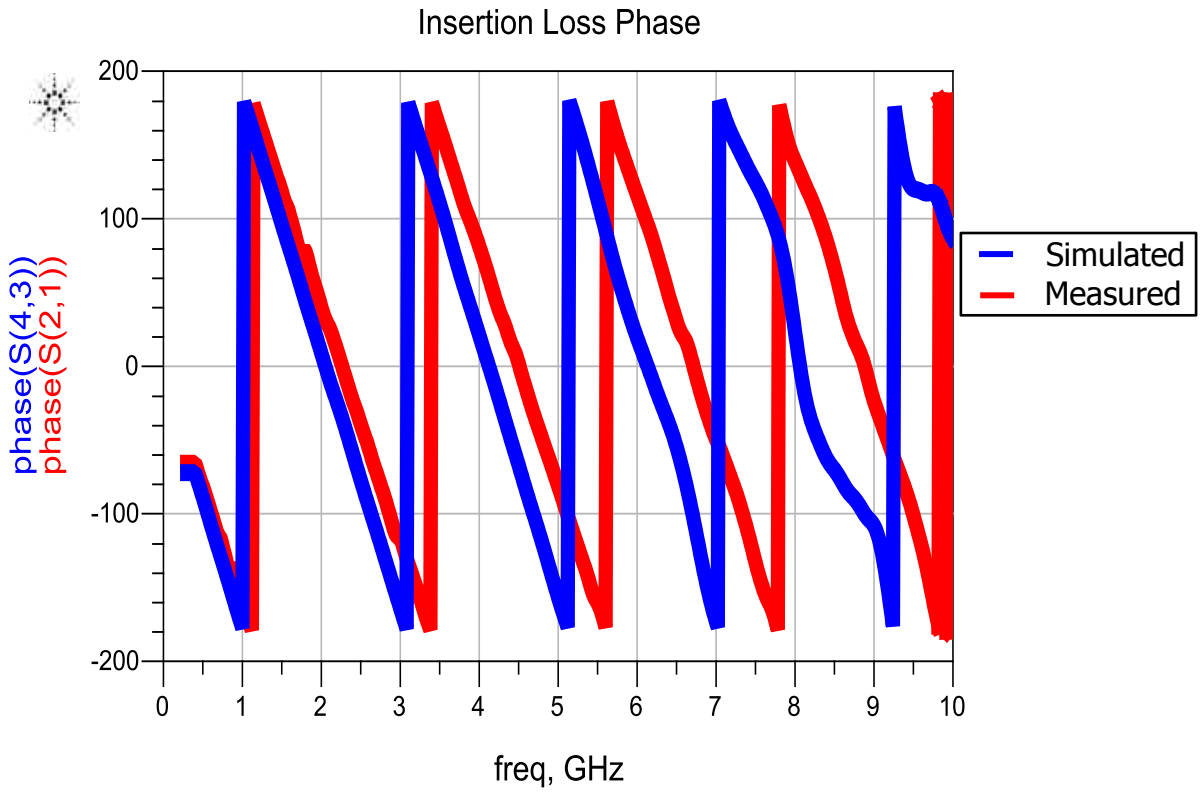

Figure 4.17 Three inch microstrip correlation of measurement to simulation using S_{21} phase

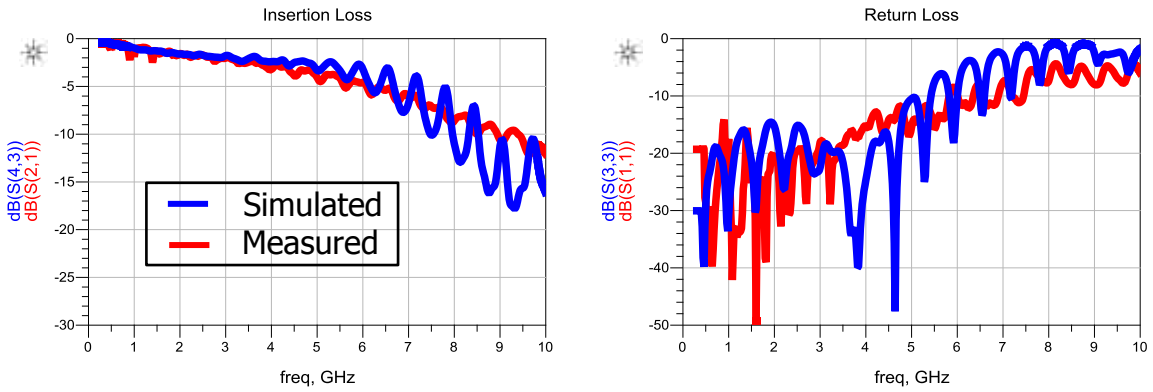

Figure 4.18 Six inch microstrip correlation of measurement to simulation using S-parameters

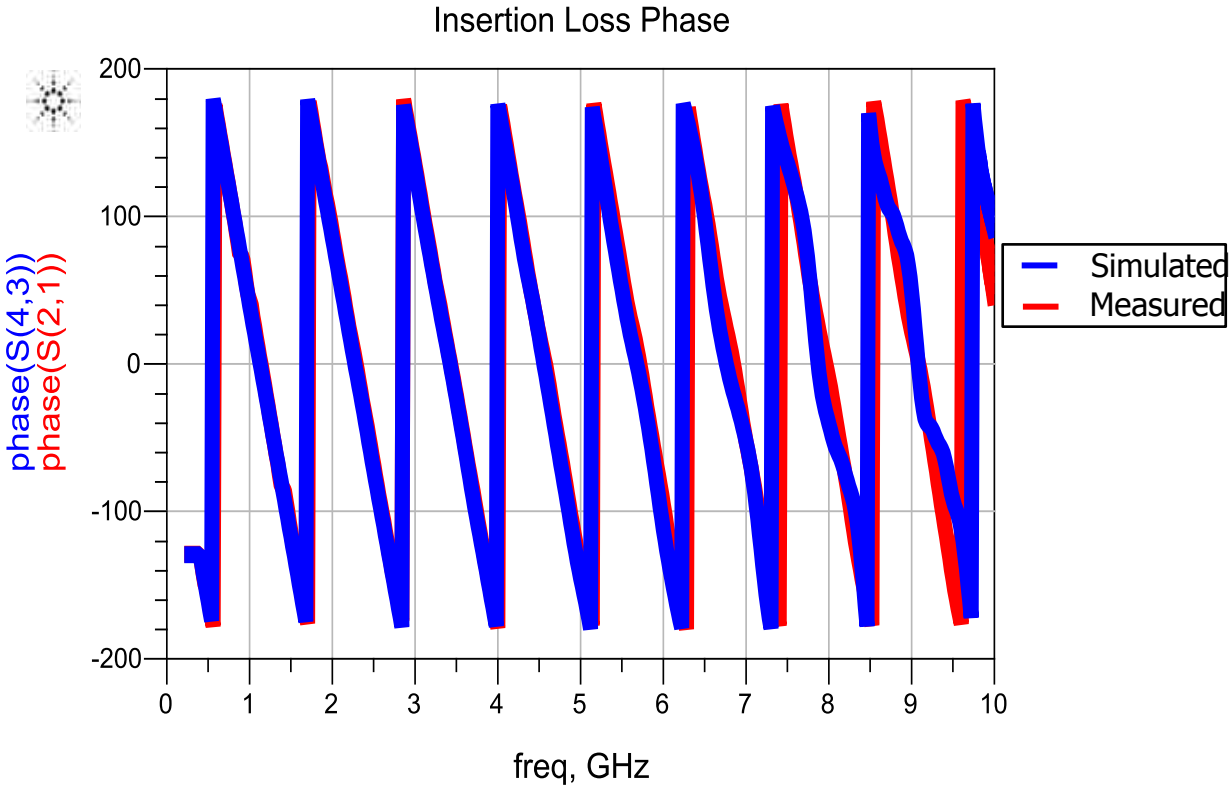

Figure 4.19 Six inch microstrip correlation of measurement to simulation using S_{21} phase

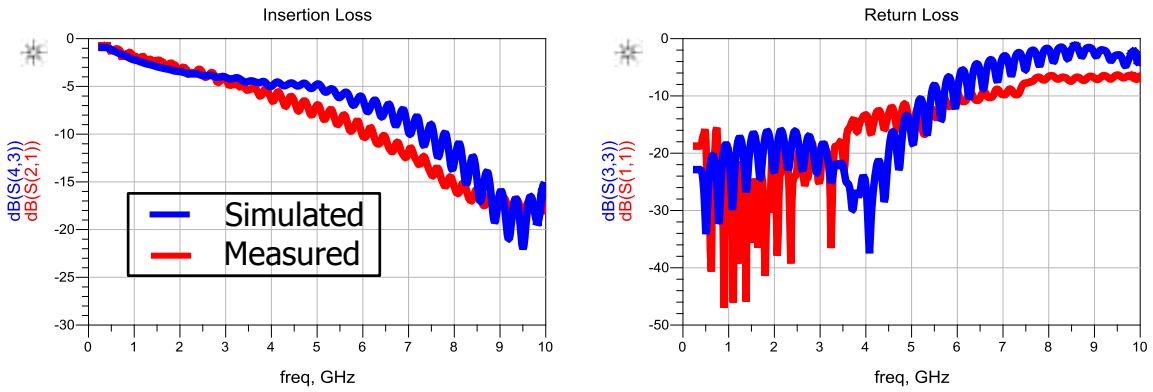

Figure 4.20 Twelve inch microstrip correlation of measurement to simulation using S-parameters

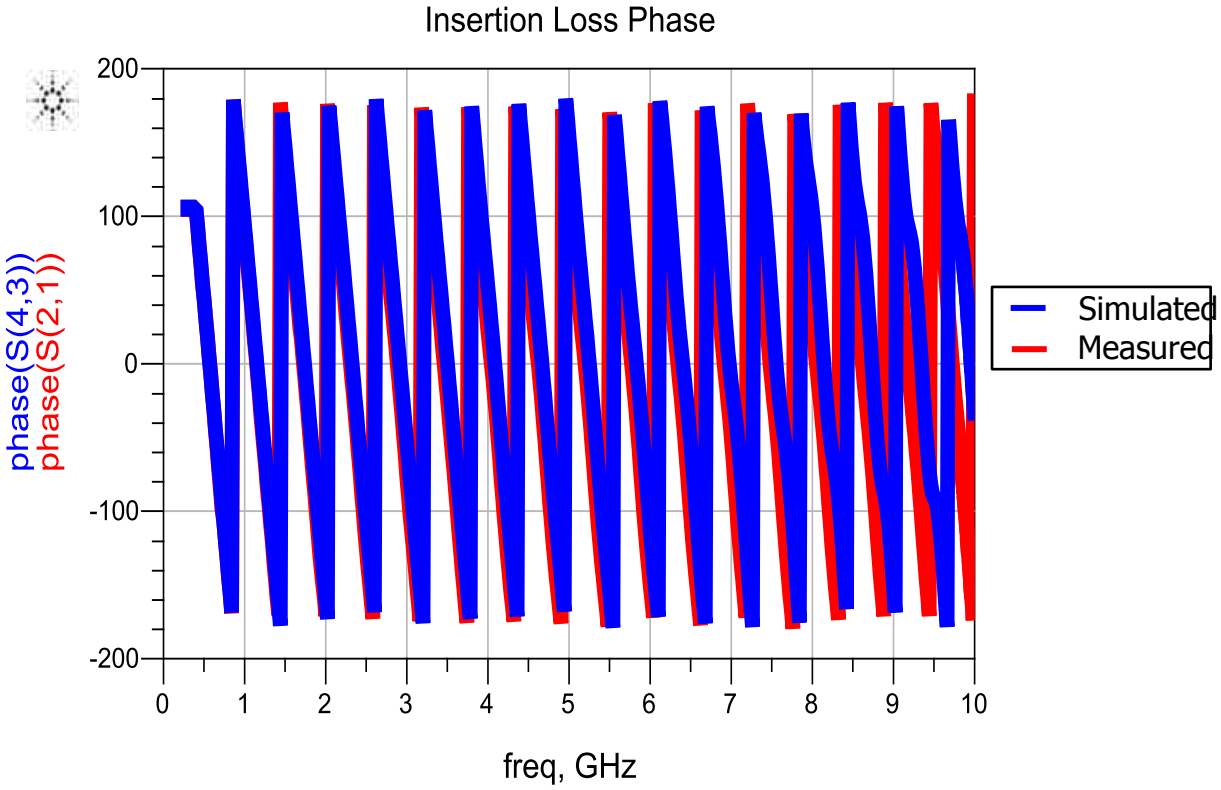

Figure 4.21 Twelve inch microstrip correlation of measurement to simulation using S_{21} phase

Next, the differential line measurement comparison will be made. The differential lines will be correlated to time-domain data. This choice was made as the differential S-parameter measurements are taken with the inclusion of an SMA adapter. This SMA adapter makes correlating to the frequency domain a challenge as it drastically changes the near end crosstalk, making the differential S-parameters look artificially lossy for the channel. As can be seen from the figures below, there is an extra snippet of transmission line and an inductive bump that come from the SMA adapter that is not included in the modeling.

Below are the three stripline cases, Figures 4.13-15, showing the differential TDR calculated from S-parameters. In general, the PCB microstrip traces correlate well to the measured results, and the cables impedance matches to about one to two ohms in the worst case correlations. In general, the resonances in the TDR match in general shape, but not in exact value. There also appears to be an extra inductive discontinuity that the models are missing. This must come from some unknown piece of geometry in the cable, which is not outlined in the design specifications.

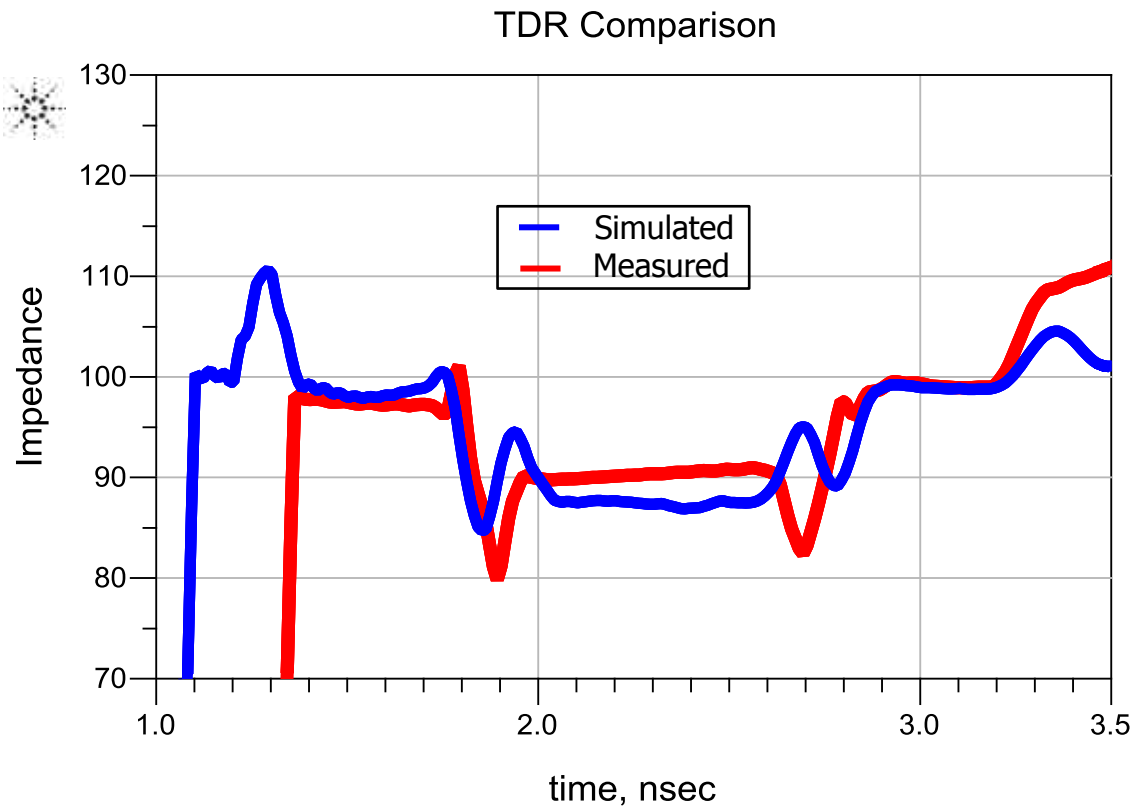

Figure 4.22 Three inch stripline correlation of measurement to simulation using differential TDR

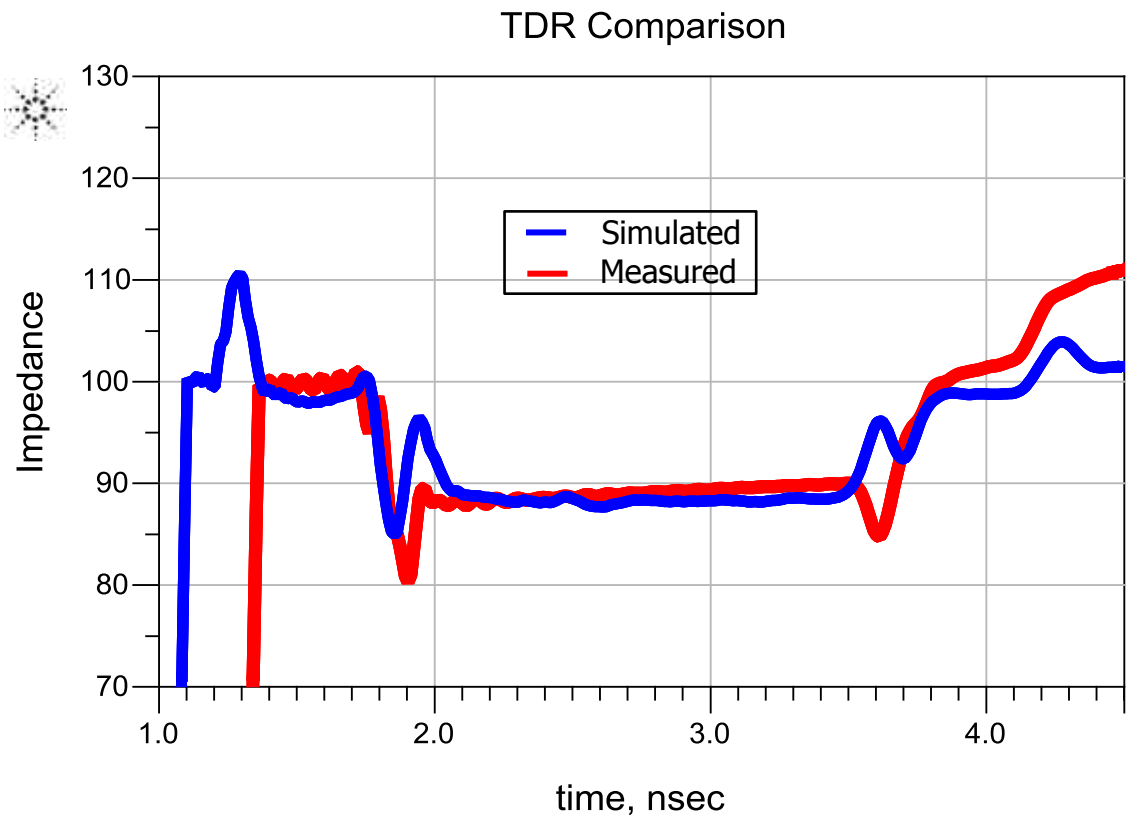

Figure 4.23 Six inch stripline correlation of measurement to simulation using differential TDR

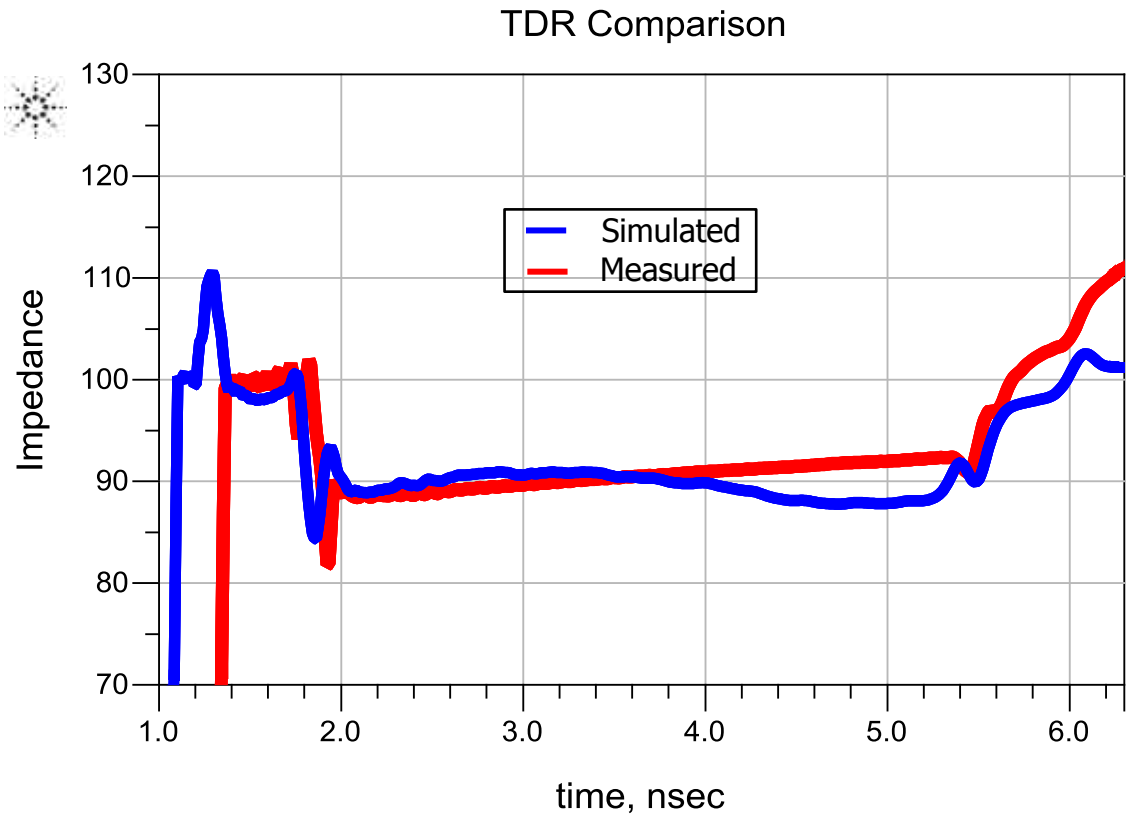

Figure 4.24 Twelve inch correlation of measurement to simulation using differential TDR

The analysis of the TDR correlation for the microstrip geometries is very similar. As can be seen from the three figures below, Figures 4.16-18, a decent match is found between the cables and microstrip on the PCB. For these models, it appears the large capacitive discontinuities appear to line up well in time and value. One unusual thing to note is the fact that the inductive bump discussed above does not appear in the microstrip geometries.

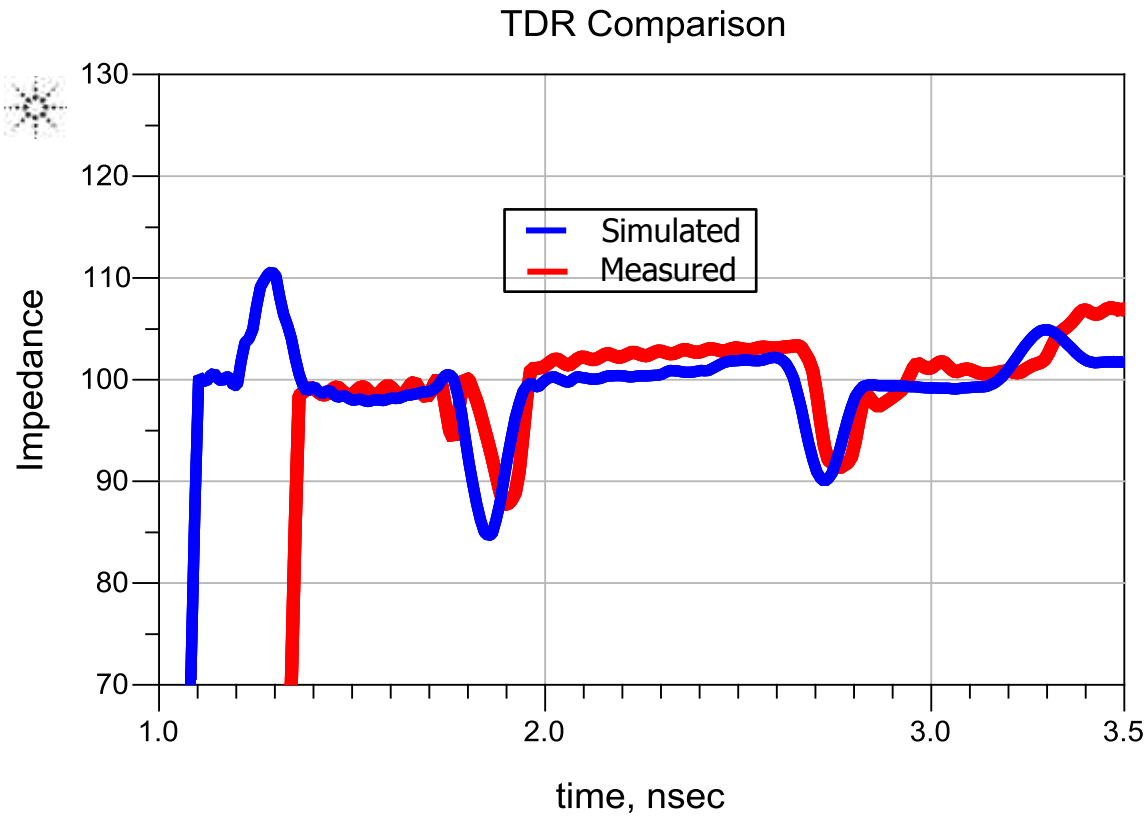

Figure 4.25 Three inch microstrip correlation of measurement to simulation using differential TDR

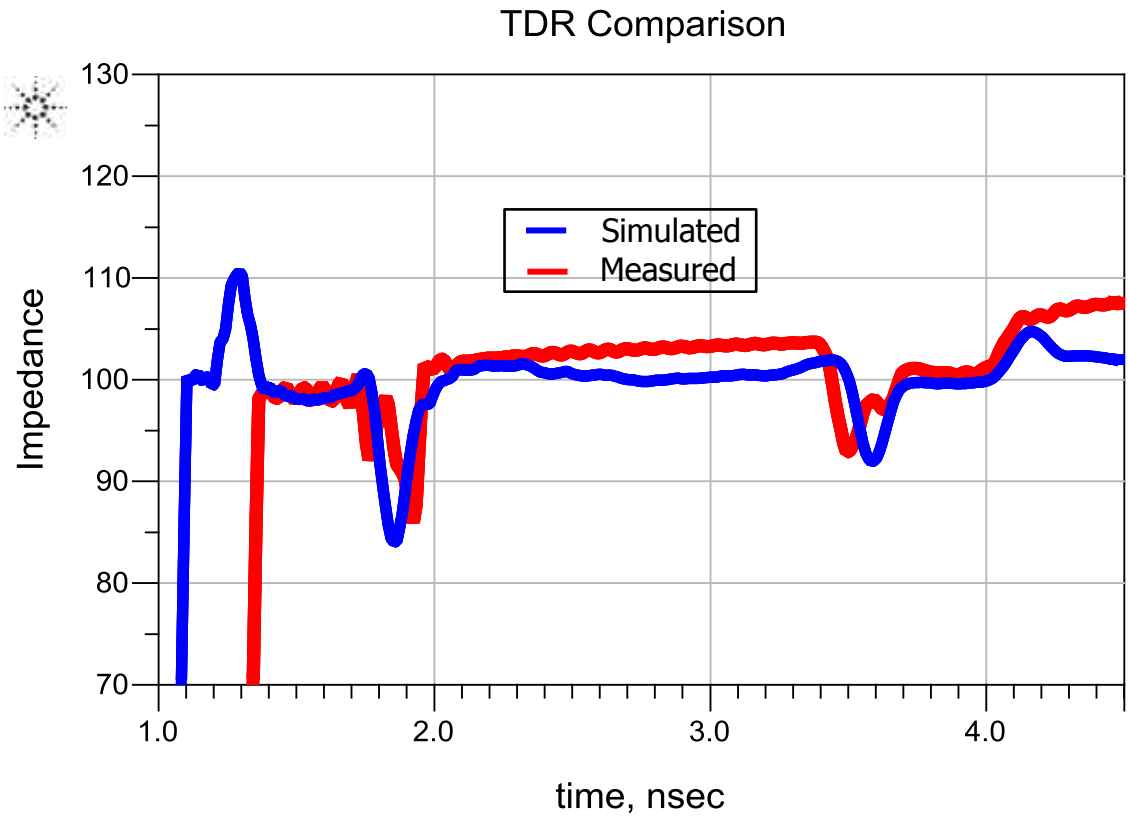

Figure 4.26 Six inch microstrip correlation of measurement to simulation using differential TDR

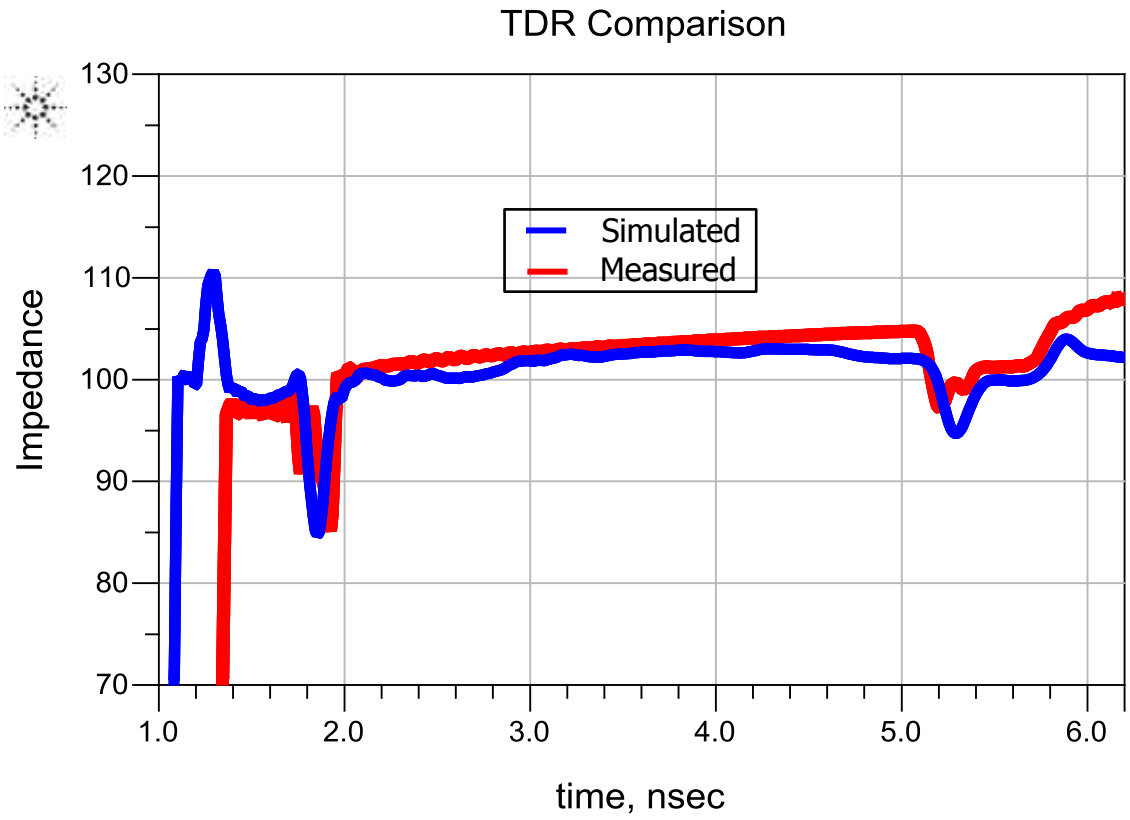

Figure 4.27 Twelve inch microstrip correlation of measurement to simulation using differential TDR

To conclude this section, a recap will be made of all the simulation results. First, the single ended stripline geometries S-parameters were matched fairly well for S_{21} losses, S_{11} loss, and S_{21} phase. For the single-ended microstrip the correlation is ok at lower frequencies and a match can be made up to about 5 Ghz for all lengths for the S-parameters. For the correlation of the differential TDR to the microstrip and stripline geometries, a good overall match is found. However for the stripline case, an extra discontinuity is found coming from some undocumented piece of geometry found in the cable

5. OPTIMIZATION OF SYSTEM

This final subsection of this thesis deals with the attempted optimization of this channel. This optimization primarily focuses on improving the performance of the transmitter and receiver. This focus was chosen as it assumes that an engineer will not have the option of modifying the physical characteristics of the system, and would have to optimize by changing the inputs and outputs to the system. As already mentioned, three optimization techniques were chosen being continuous time linear equalization (CTLE), transmitter de-emphasis, and decision feedback equalization (DFE). These three techniques were simulated in Agilent's Advanced Design Systems component based modeler using the measured and simulated S-parameters for the all the many design variations. In this section, the details of the simulation setup for each of the various techniques will be reviewed, followed by the results and a comparison of the optimized and non-optimized results.

The CTLE optimization can be performed a number of different ways. Passive CTLE can be generalized to the well-known concept of band-pass filtering. This means that CTLE on the receiver side of this system can be describe completely by use of a pole-zero form equation of its transfer function. For a bandpass filter, this pole-zero equation will have one unique zero and two unique poles [7]. In this study, a component highpass filter was chosen as shown in Figure 5.1. Formulations were then found that relate the resistance and capacitance values to the low and high frequency gain and the peaking frequency. By choosing the Nyquist frequency of the swept data rates as the peaking frequency, the optimal component values for each data rate can be found. Data rates were then swept for three, six, and eight Gbps for each of the design variations.

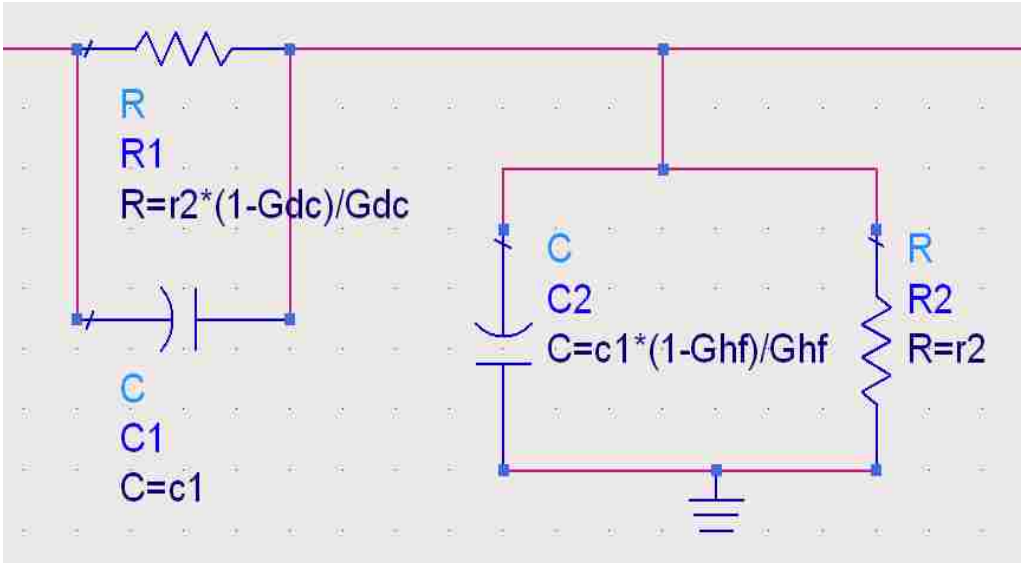

Figure 5.1 Schematic of circuit based passive CTLE implementation

The setup for the transmitter de-emphasis is very straightforward in the software used. Transmitter de-emphasis uses the well know concept of FIR filtering to create a time domain waveform that increase certain frequency components. The main goal in de-emphasis is to reduce the ISI that is caused by the impulse response tail. The emphasis works by effectively subtracting out the long tail component of the last symbol received. For this study a two tap FIR filter was chosen due to its prevalence in industry. Because de-emphasis is used, the filter coefficients will all be positive in time, meaning no delays before the input to the FIR filter, simplify the design. The FIR response coefficients are easy to choose and the coefficients of 0.9 and -0.1 were chosen. These coefficients have similar effects at the various data rates, and therefore do not need to be optimized for each data rate. As the CTLE simulation above, this simulation was performed for all the design variations of both the simulated and measured s-parameters for data rates of three, six, and eight Gbps.

Decision feedback equalization was implemented using the built-in optimization feature in ADS. ADS finds the best fit filter coefficients for the FIR filter used in the DFE. This is done through a recursive least means square algorithm that's fits the coefficients to produce the least mean error of the desired equalizer and the actual equalizer. This can be done because the sent signals are known and therefore the received signals can be analyzed and values for the coefficients can be found in a pre-processing stage. For this study, a 2 tap DFE was used and all design variations were simulated using both the simulated and measured S-parameter data all being optimized via the ADS software.

First, the eye diagrams should be inspected for cases without any optimization. This will establish a baseline by which improvements can be extrapolated. Below, eye diagrams are shown for the microstip and stripline cables, for all length variations with three, six, and eight Gbps data rates. A rise and fall time was chosen such that they are one third of the total UI for each data rate. Eye diagrams are simulated through the use of the measured and simulated single ended S-parameters.

For both the microstrip and stripline geometries, shown in Figure 5.2 and Figure 5.3, it can be seen that the eye diagrams for the measured S-parameters are fairly good. Having a good eye heights and widths. This suggests that these two lengths could be used for each of these data rates. However, for the 12'' cable length for both geometries with cannot see an eye opening at all. This means that we cannot expect the 12'' cable to perform well for any of the data rates, and to consider these data rates some optimizations need to be incorporated. The simulated Eye Diagrams perform much worse for these eye diagrams, this is due to the fact that we have more limited bandwidth for the simulated data, and that the simulated data appears worse than the measured data in the s-parameters.

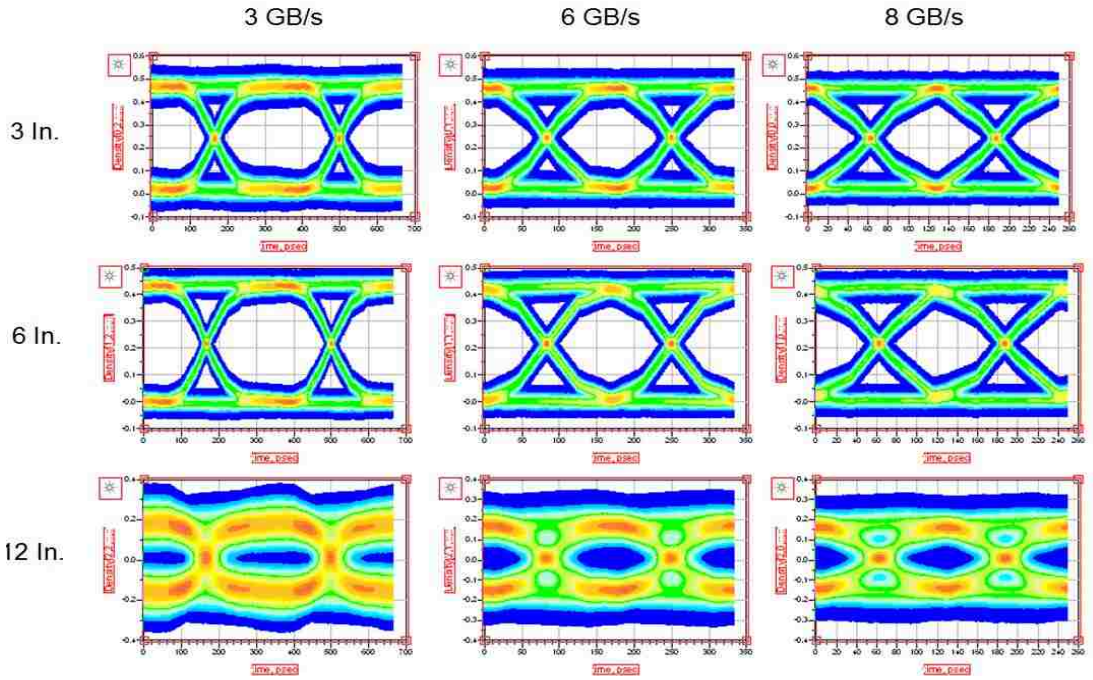

Figure 5.2 Non-optimized eye diagrams for all stripline design variations and data rates

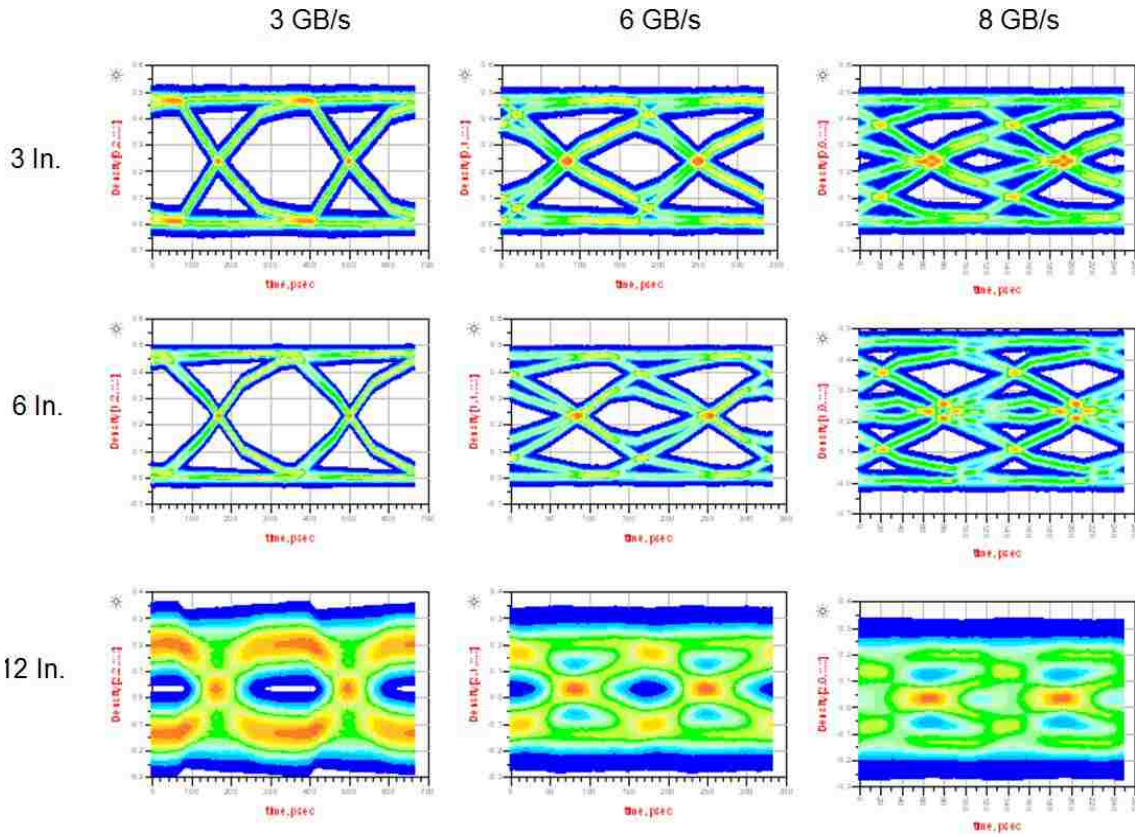

Figure 5.3 Non-optimized eye diagrams for all microstrip design variations and data rates

First, the passive CTLE optimiizatoin will be demonstrated. As stated above, a component based bandpass filter was chosen for this study. This is beneficial as it is simple to implement both practically and in the simulation software. Equations were derived based on the transfer function of the circuit that allows for the choice of low frequency gain and peaking frequency. This component was optimized such that the peaking frequency is very near the nyquist frequency and DC gain chosen such that the losses seen in the low frequency region of the circuits transfer function do not go below -2dB. Below are the reults, Figure 5.4 and Figure 5.5, of the passive CTLE implementation. Overall, we do not see significant improvements for the measured results for the stripline geometry. This is due in large part to the fact that the three

and six inch cables already perform very well, so very small improvements do not make as large of an impact. And also the twelve inch case does so poorly that small performnace enhancements do not improve the eyes in a meaningful way. In the microstrip design, we can see some performance improvement for many of the eyes from a reduciton in ISI. In the six GBPS cases and wee see that the double crossings have almost dissapeared.

Passive CTLE may not be a good choice for the stripline channel. This channel is already fairly lossy so ISI will not be a significant issue seen in the eye diagrams. This type of equalization my be better used for channels with flatter responses, where there is a greater need for the filtering of high frequency losses. Also, it would be more advantageous to use an active CTLE implemenation. This would make it such that the, the lower frequency components do not receive a great amount of loss, and would provide some gain at the Nyquist frequency. The microstrip design could possibly implement CTLE to increase the performance of some data rates, and could be considered useful.

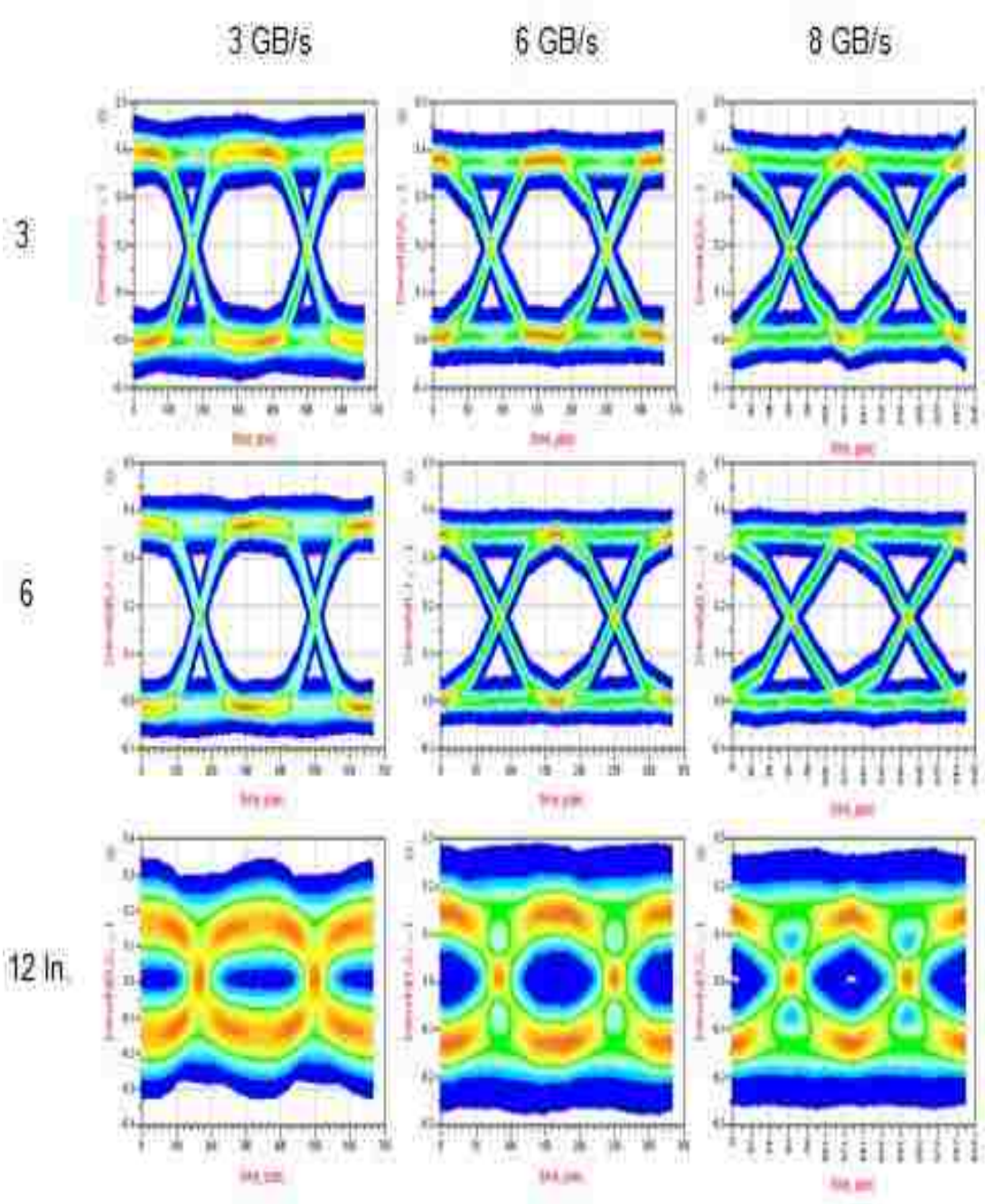

Figure 5.4 Eye diagrams for all stripline design variations and data rates using CTLE

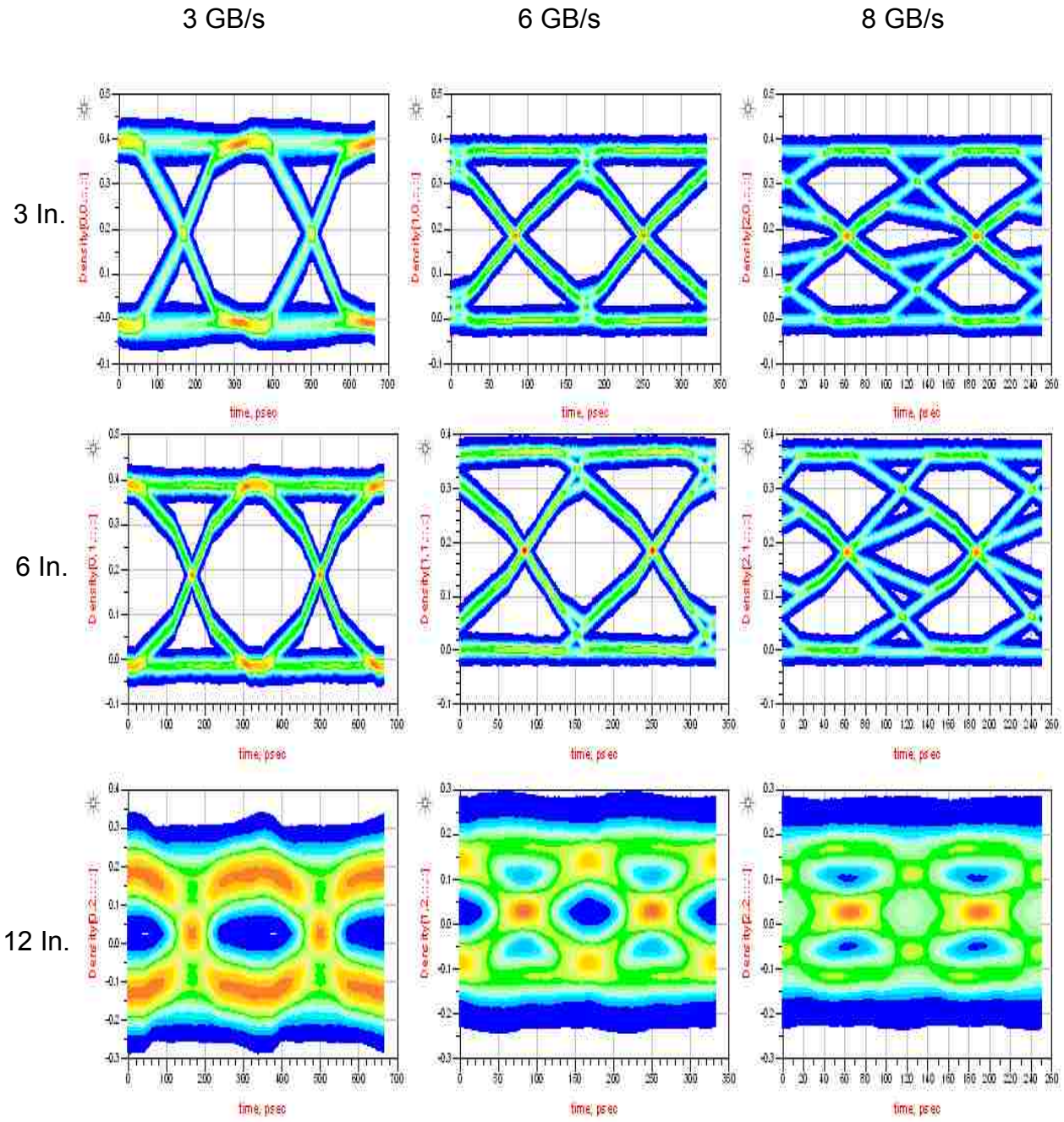

Figure 5.5 Eye diagrams for all microstrip design variations and data rates using CTLE

Transmitter de-emphasis was implemented via Ads tools. In this toolbox, one can set the tap coefficients to create transmitter de-emphasis. In this study two-tap transmitter de-emphasis

was chosen using co-efficient of 0.9 for C0 and -0.1 for C1. The absolute sum of these is equal to one making this a passive implementatoion. These particular values were chosen as they are typical for two tap de-emphasis. Shown below are the results, Figure 5.6 and Figure 5.7, of this optimization. Overall, the performance of the stripline design stays fairly nominal, only slightly improving or detioriating. If different coeeficients are chosen, for example 0.75 and -0.25, a slight increase in performance can be seen in the 12 inch cables. This increase is pretty small and results in siginificant ISI found for the three and six inch cables' eye diagrams for all three data rates. Once again, the microstrip design is improved with a decrease in ISI for the six Gbps data rates and even for the eight Gbps data rate for the three inch cable.

To summarise, it can be seen that the optimization does very little to improve the performance for the sripline cables, for the same reasons mentioned for the CTLE implementation. However, this could be a reasonable choice for the improvement of the three inch and three inch cables for data rates of six Gbps and even eight Gbps for the three inch case.

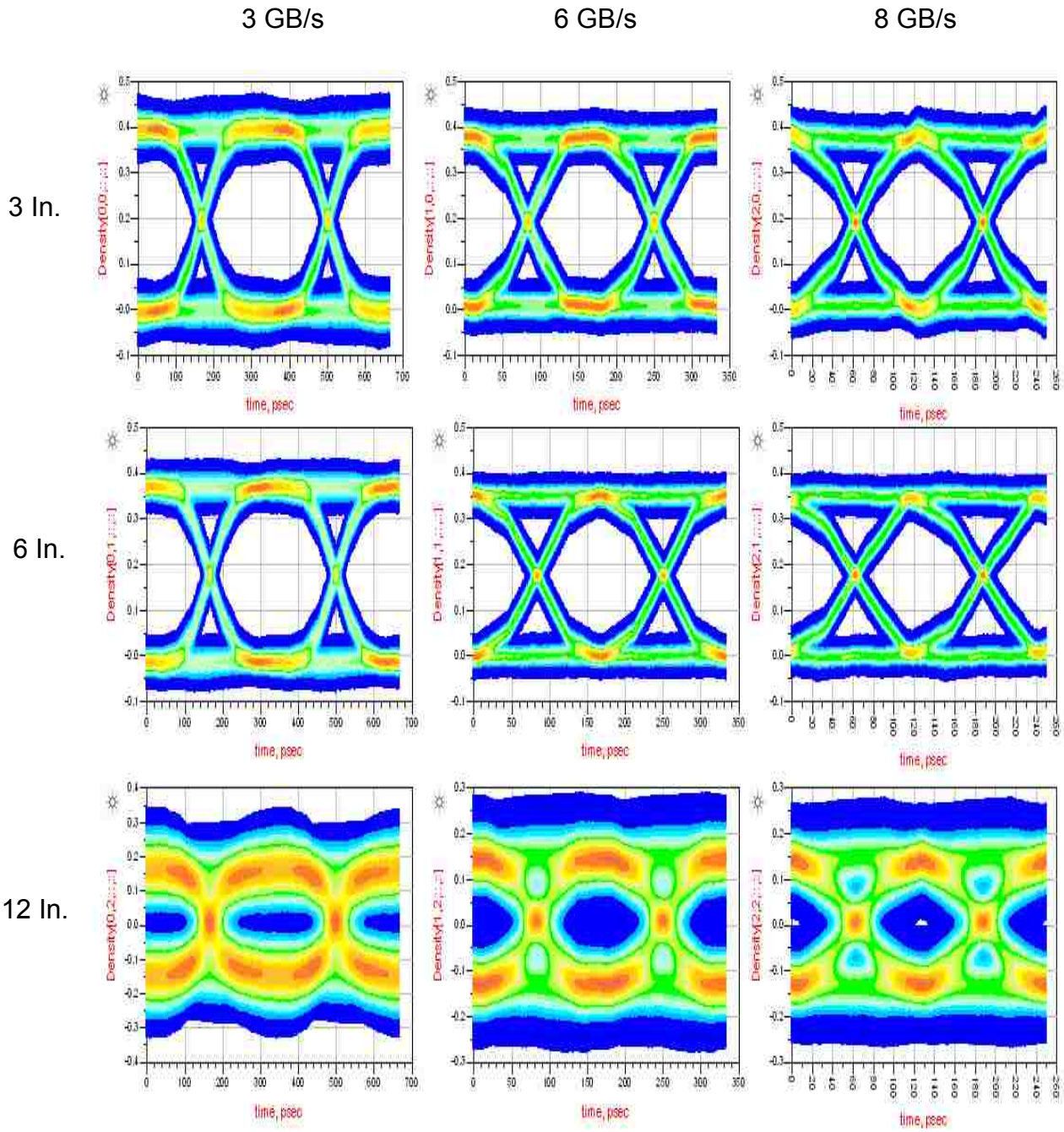

Figure 5.6 Eye diagrams for all stripline design variations and data rates using transmitter de-emphasis

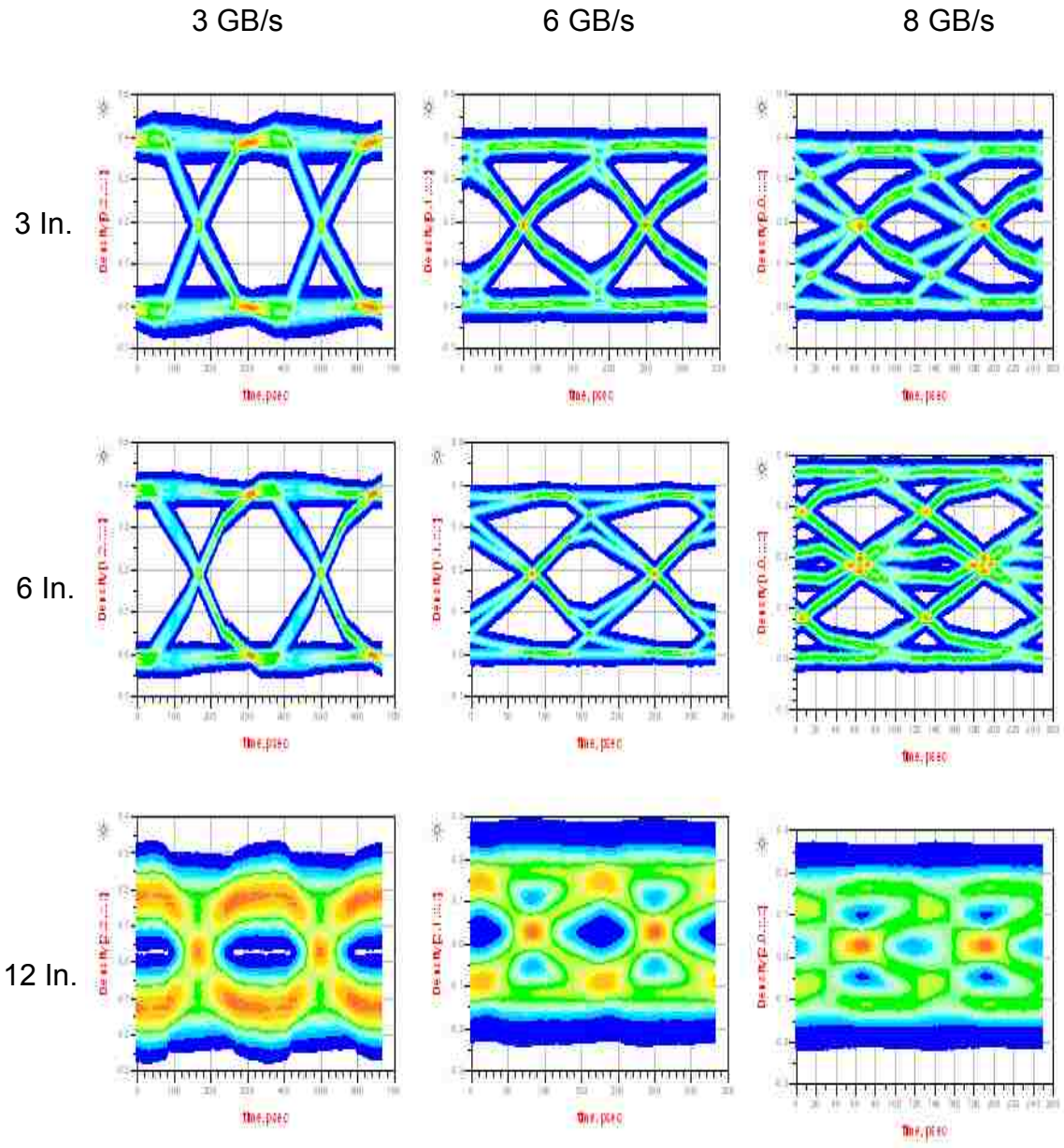

Figure 5.7 Eye diagrams for all microstrip design variations and data rates using transmitter de-emphasis

The DFE optimization was performed using both the measured and simuatled S-parameters. DFE can be optimized through the algorithms discussed above in ADS. For this study, a two tap optimized DFE is used. From Figure 5.8 and Figure 5.9 below, we can see the DFE optimization results. First, it should be noted that there now exists some odd clipping. This

clipping comes from the non-linear sampling in the DFE circuit, which occurs when the symbol decision is made. Overall, the eyes have improved relative to the non-optimized case. For the stripline cables, these changes are pretty small and would probably not warrant the use of such a complicated system. It can be seen that the microstrip does improve significantly in some cases, reducing a lot of ISI. For the six and eight Gpbs data rates we may be able to use both cables, albeit the six inch cable may not be preferable.

In general, the DFE algorithm is not a good choice for either of these design variations but for different reasons. For the stripline case, it does very little to improve the overall performance of the system. While the microstrip data eyes do improve, they do not improve much more than cheaper and easier to implement methods. As a result, these other methods would make for a much better diesign decision.

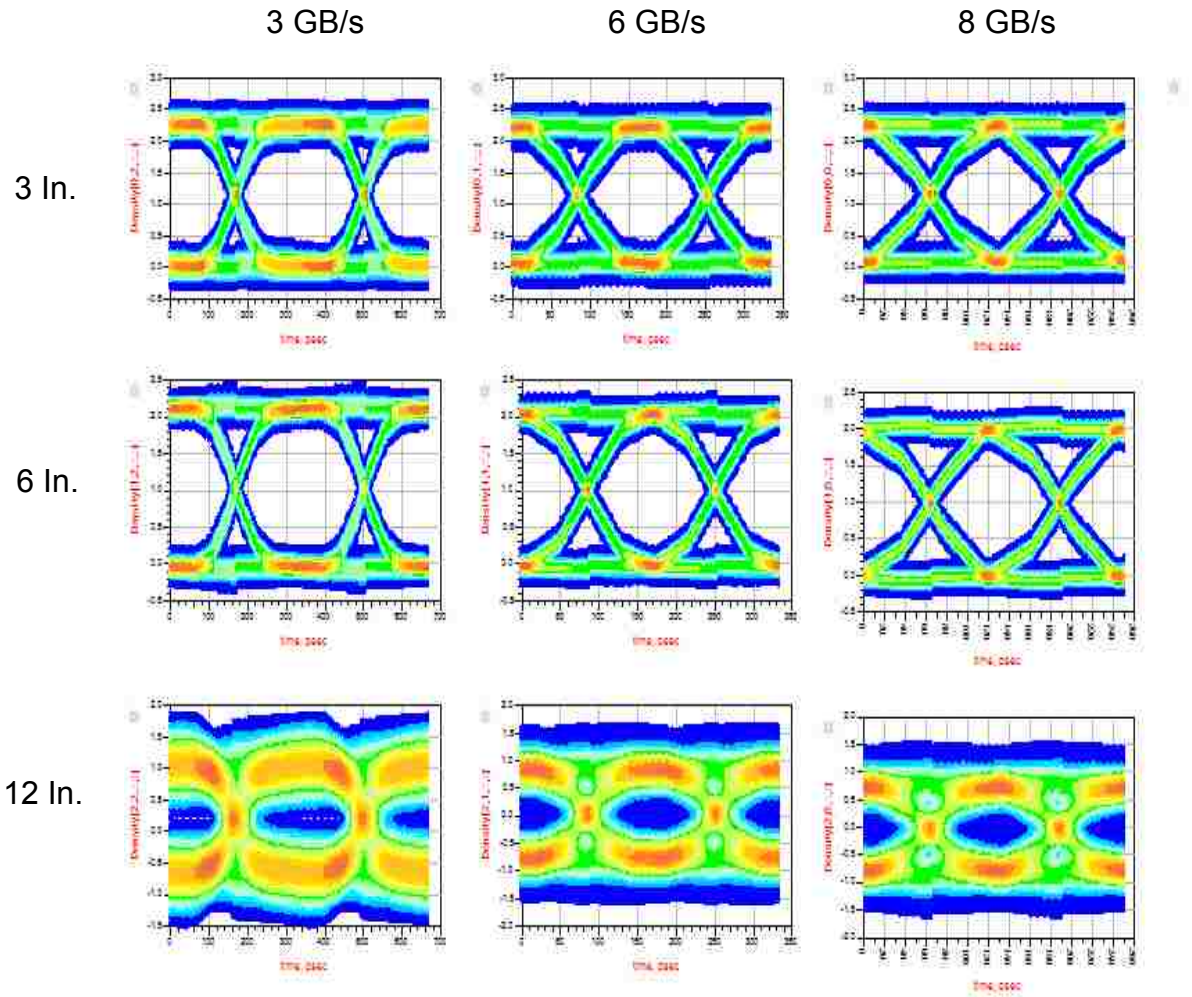

Figure 5.8 Eye diagrams for all stripline design variations and data rates using DFE

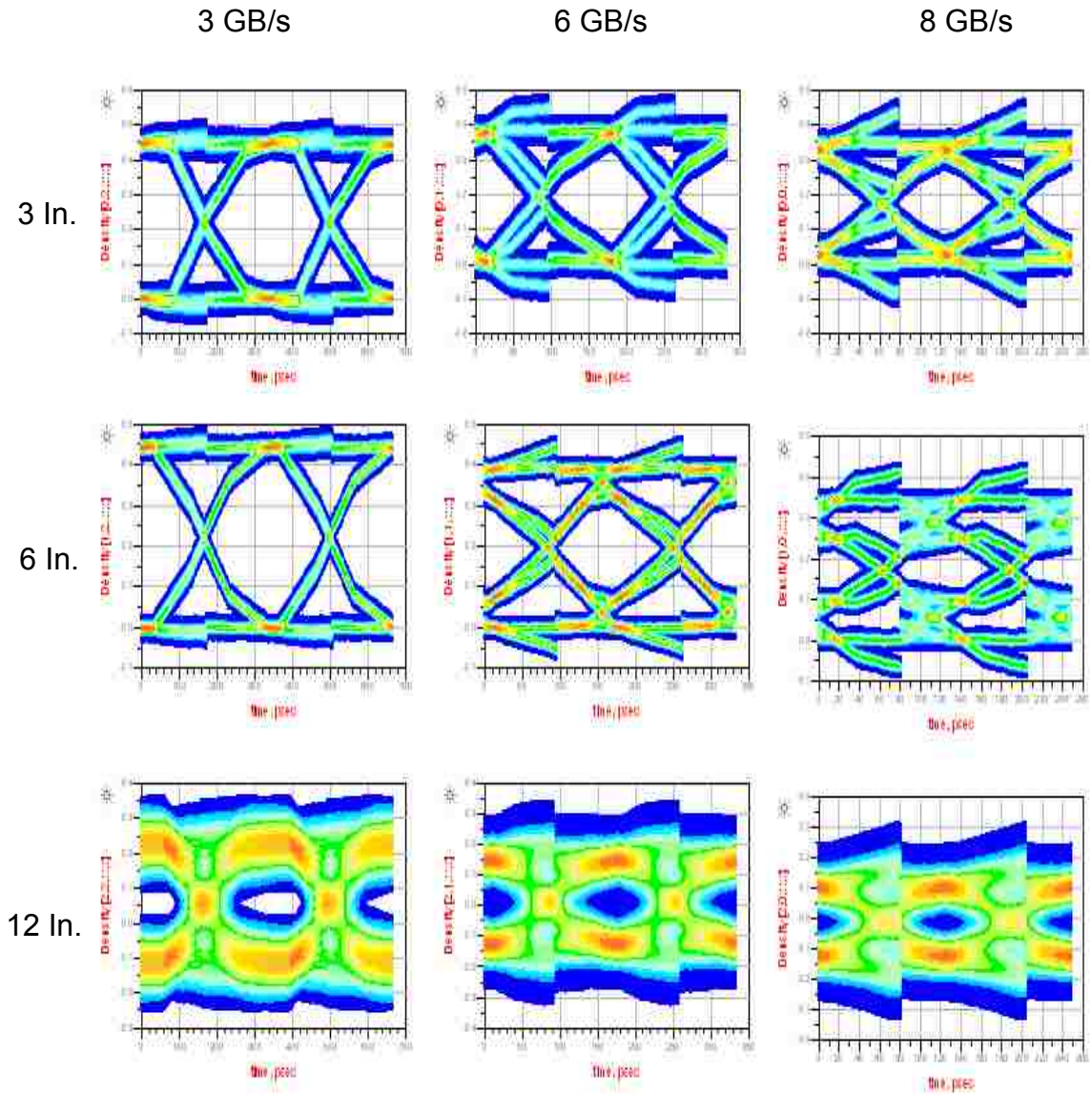

Figure 5.9 Eye diagrams for all microstrip design variations and data rates using DFE

To conclude this section, a recap of the findings will be given which will be segmented by the two geometries. For the stripline geometry, there does not seem to be a great amount of optimization that is possible. For all three techniques attempted, we can see miniscule improvements in the best case and even some detriments in some cases. This is due to the good

design of the three and 6 inch cables, which work well without any optimizations. And because of the ill designed twelve inch cable which seems hopeless to improve. The microstrip geometry provides more interesting analysis. In most cases, the optimizations seem to improve performance to some degree. This is a result of increased ISI found in the design. The CTLE would probably be the best choice for optimizing this design as it is the easiest to implement and least expensive. However, if higher data rates are needed, de-emphasis should be chosen.

6. CONCLUSION

This thesis has outlined the measurement, simulation, and optimization of a low cast PCB to PCB system using a flex cable. This system includes several design variations of flex cables, including 3 different lengths: three, six, and twelve inches, two geometry types: microstrip and stripline, and two signaling types: single ended and differential. As well as studying the effect of these many design variations, differing data rates are also studied and then optimized using equalization techniques. To conclude this study, a summary of each of the subsections discussed above and the results therein will be presented.

The study began by taking a set of measurements for the system. These measurements were then used to characterize the system and to estimate the digital performance. Each of the design variations were measured in the time and frequency domain using VNA and TDR equipment. These results give an indication of how well the system may perform in a high speed digital applications. As has been said before, increasing the length of the flex cables increases the losses at higher frequencies, and as a result performance will be degraded. Also, it has been shown that the single-ended microstrip design is not designed well in terms of characteristic impedance. This also being the case for the differential stripline variations.

Next, an attempt to build a model in both full-wave and quasi-static solvers was attempted for each of the design variations. These results are then compared to the measurement, to see how well they correlate. From above, it can be seen that many results match well. However, there can be some improvements especially for the single ended microstrip line as it is matched by S-parameter data.

Finally, an optimization of performance was attempted through the techniques of transmitter de-emphasis, continuous time linear equalization, and decision feedback equalization. The conclusions drawn from this attempt is that, overall, the system is better optimized through

the use of CTLE and TX de-emphasis due to their decreased cost and easier implementation., It was also seen that that 12’’ design variations are too lossy to be effective at the data rates explored.

In this report, it has been shown how a low-cost system can be studied and improved in terms of digital performance. This study has outlined how, within limitations, a systems performance can be improved through the use of equalization techniques.

7. BIBLIOGRAPHY

[1] "Hirose," [Online]. Available: http://www.hirose.co.jp/cataloge_hp/ed_FH41_20140305.pdf. [Accessed 20 Januaruy 2014].

[2] Nicomatic, "Nicomatic," [Online]. Available: http://www.nicomatic.com/data/files/1ff8a7b5dc7a7d1f0ed65aaa29c04b1e/22102014113124-nicomatic-ffc-cables--jumpers-catalogs.pdf. [Accessed 2014 December 2014].

[3] Agilent, "Agilent," [Online]. Available: http://cp.literature.agilent.com/litweb/pdf/5965-7917E.pdf. [Accessed 12 January 2014].

[4] Agilent, "Agilent," [Online]. Available: http://literature.agilent.com/litweb/pdf/5966-4855E.pdf. [Accessed 20 December 2014].

[5] S. Hall and H. Heck, Advanced Signal Integrity for High Speed Digital Designs, Wiley-IEEE Press, 2009.

[6] "CST," [Online]. Available: https://www.cst.com/. [Accessed 20 December 2014].

[7] S. Palermo, "Texas A&M," [Online]. Available: http://www.ece.tamu.edu/~spalermo/ecen689/lecture18_ee689_rx_fir_ctle_eq.pdf. [Accessed 20 December 2014].

[8] S. Palermo, "Texas A&M," [Online]. Available: http://www.ece.tamu.edu/~spalermo/ecen689/lecture19_ee689_rx_dfe_eq.pdf. [Accessed 20 December 2014].

[9] Keysight, "Keysight Technologies," [Online]. Available: http://www.keysight.com/en/pc-1297113/advanced-design-system-ads?cc=US&lc=eng. [Accessed 20 December 2014].

[10] Tektronix, " Tektronix," [Online]. Available: http://www.tek.com/sites/tek.com/files/media/media/resources/80E00-Electrical-Sampling-Modules-Datasheet_85W-13497-14_0.pdf. [Accessed 20 December 2014].

[11] Agilent, "Agilent," [Online]. Available: http://emlab.uiuc.edu/ece451/appnotes/TRL_2.pdf. [Accessed 20 December 2014].

[12] Agilent, "Agilent," [Online]. Available: http://literature.cdn.keysight.com/litweb/pdf/N5224-90001.pdf. [Accessed 20 December 2014].

[13] Hirose, "Hirose," [Online]. Available: http://www.hirose-connectors.com/connectors/3d_download01.aspx?T1=FH41. [Accessed 20 December 2014].

8. VITA

Kancy Robison was born in Mattoon, Illinois in 1988. Moving to Salem, Missouri in 2001, where he attended high school at Salem Senior High School. He received his bachelor's of science in electrical engineering at the Missouri University of Science and Technology. In May, 2015, he received his master's in electrical engineering.